Receive Beamforming Schemes to Mitigate Inter-Operator Pilot Contamination in RIS-Aided MIMO Networks

DOĞA GÜRGÜNOĞLU[1], ZİYA GÜLGÜN [1], EMIL BJÖRNSON[2] *(Fellow, IEEE)*, AND GABOR FODOR[2,3] *(Fellow, IEEE)*

[1]Communication and Information Technologies Sector, Aselsan Inc., Ankara, 06800 Türkiye
[2]School of Electrical Engineering and Computer Science, KTH Royal Institute of Technology, Stockholm, 100 44 Sweden
[3]Ericsson Research AB, Stockholm, 164 80 Sweden

CORRESPONDING AUTHOR: Doğa Gürgünoğlu (e-mail: dogagurgunoglu@gmail.com).

This study is supported by EU Horizon 2020 MSCA-ITN-METAWIRELESS, Grant Agreement 956256. E. Björnson is supported by the FFL18-0277 grant from the Swedish Foundation for Strategic Research. G. Fodor was supported by the Swedish Strategic Research (SSF) grant for the FUS21-0004 SAICOM project.

ABSTRACT When reconfigurable intelligent surfaces (RISs) are integrated into cellular networks, they can give rise to inter-operator pilot contamination, severely degrading network performance. While combating this effect is possible by orthogonalizing the RIS configurations, it requires inter-operator coordination and limits the degree of configuration freedom per RIS. Therefore, in this work, we explore the use of receive beamforming to mitigate inter-operator pilot contamination in RIS-aided multiple input multiple output systems, where two operators share infrastructure and deploy RISs to enhance network coverage. We focus on uplink channel estimation and data transmission and propose a method in which the base stations (BSs) apply a novel kind of receive beamforming to suppress pilot-contaminated interference. We compare our proposed method with a previous RIS orthogonalization approach and another approach that does not eliminate inter-operator pilot contamination by formulating two schemes. In Scheme 1, the BS beamforms towards its intended channel without nulling the interfering channel while orthogonal RIS configurations mitigate pilot contamination. In Scheme 2, the BS nulls the interfering channel, removing the need for orthogonalized RIS configurations and thereby halving the number of pilots. In the baseline scheme, the BS uses the same beamformer as in Scheme 1 and the same RIS configurations as in Scheme 2, hence does not eliminate pilot contamination. We assess the performance of both schemes under different channel conditions, in terms of channel estimation mean square error and capacity bounds with imperfect channel state information. Our numerical results indicate that Scheme 2 offers a superior rate at high signal-to-noise ratios (SNRs) due to fewer pilots and comparable channel estimation accuracy, while Scheme 1 performs better at very low SNRs due to capturing more energy. However, the reduced number of pilots in Scheme 2 makes it a favorable choice for practical systems, with minimal performance loss at low SNR. Overall, the proposed beamforming approach effectively mitigates inter-operator pilot contamination.

INDEX TERMS Channel estimation, Pilot contamination, Reconfigurable intelligent surface, Receive beamforming, Null forming, Spectral efficiency.

I. INTRODUCTION

In the past few decades, multiple-input multiple-output (MIMO) systems have changed the way we communicate [1], [2]. As they became prevalent due to the large-scale deployments by multiple operators, they made a revolutionary impact on the achievable performance of mobile broadband services [3]. Thanks to the multiple antennas, wireless channels gained multiple spatial degrees-of-freedom allowing for spatial diversity and multiplexing schemes that improve signal quality and enable to serve multiple users using fewer resources over time and frequency [4]. In addition, the presence of multiple antennas gave rise to an effect called channel hardening, which made the channels with more antennas less random, resulting in lower outage probabilities

and hence increased reliability [5]. As a result, MIMO technology became a game changer in communication systems allowing for higher spectral efficiency and increased throughput. As a result, it allowed data-heavy use cases – such as high-quality audio and video streaming services – to become a reality. In the 5G era, MIMO has evolved into massive MIMO with a larger number of antennas, where the beamforming and spatial multiplexing capabilities of MIMO systems can be further utilized [6]–[8].

Receive beamforming techniques for interference cancellation and performance enhancement have been extensively studied in various wireless communication scenarios. The maximum ratio combining (MRC) introduced in [9] and [10] determines the beamforming vector that maximizes the received power for a particular channel. This approach focuses the receiver beam toward the incoming signals and adjusts its focus according to the signals' power levels. However, MRC does not eliminate interfering signals, which proves to be problematic when the interfering signals are closely aligned with the intended signals. The concept of null forming is introduced in [11] to overcome this problem. In the context of modern wireless communication systems involving MIMO channels, collecting the maximum power from a channel involves beamforming according to the dominant singular vectors of the channel of interest. In contrast, null forming involves orthogonalizing the beamforming vector to the singular vectors of the interfering channel corresponding to its non-zero singular values. While this approach eliminates interference, it sacrifices the power collected from the intended channel depending on how closely the intended signal and the interference are aligned. Since both MRC and null forming depend on the channel responses, they rely on high-quality channel estimates. It is typical to see a tradeoff between the two goals and minimum mean squared error (MMSE) methods are developed to achieve a balance between them.

While the benefits of massive MIMO systems are numerous and obvious, they have to deal with a potential problem that may limit their performance in practice, namely pilot contamination [12]. When multiple users use the same pilot sequences simultaneously in the same band, due to the limited channel coherence time, the base station (BS) cannot distinguish their channels. This typically results in poor channel estimates and extra beamformed interference from or towards the user equipments (UEs) that reuse the same pilot sequence. Therefore, pilot contamination adversely affects the coherent reception of data, and methods to mitigate pilot contamination –including adaptive pilot reuse, power control, user grouping, multi-cell coordination, and coded random access techniques– have been widely studied in the communication literature [6], [12]–[15].

As recent works on the techno-economic aspects of communication networks indicated [16]–[19], site and infrastructure sharing helps mobile network operators (MNOs) to reduce their capital and operational expenditures. For example, reference [17] concluded that infrastructure sharing between MNOs—which can involve mast or site sharing or co-locating cellular BSs on the roof of a building—in rural or urban environments may significantly reduce expenditures. The level of cost savings due to infrastructure sharing depends on the revenue per user, service adoption rate and the amount of existing site infrastructure.

Reconfigurable intelligent surfaces (RISs) are emerging as a promising technology for enhancing wireless communication systems. RISs consist of numerous controllable reflecting elements that can manipulate electromagnetic waves, enabling functions such as reflective beamforming and wireless power transfer [20]. These surfaces can be reflective, transmissive, or hybrid, operating at high frequencies to overcome signal attenuation and blockage [21], [22]. RISs offer potential applications in improving spectrum efficiency, coverage extension, and energy efficiency for wireless communications, as well as RF sensing for security and smart spaces [23]. Recent advancements include wave-controlled architectures that reduce hardware requirements while maintaining adaptability [24].

Despite their potential, RISs face challenges in implementation and integration with existing systems. One of the main reasons is the increased complexity of channel estimation due to the presence of RISs. The channel dimensions are multiplied by the number of RIS elements, hence the number of pilot transmissions to estimate the channels increases significantly [25]–[28]. The RIS must change its configuration to explore all channel dimensions [29], [30]. In addition, the path loss of the reflected path through a RIS is proportional to the multiplication of the path losses to and from the RIS [31], so a larger surface is needed to achieve a decent signal-to-noise ratio (SNR) improvement.

Another hurdle in front of integrating RISs into practical communication systems is a newly discovered phenomenon called inter-operator pilot contamination, which arises from multiple operators sharing sites utilizing RISs that are relatively close to the shared site (Figure 1). When a user's signal gets reflected from the other operator's RIS towards the BS, the additional reflection path cannot be resolved from the intended reflection path, resulting in inter-operator pilot contamination. The main difference between traditional pilot contamination and inter-operator pilot contamination is that the former is caused by different users using the same pilot sequence in the same band, while the latter is caused by the reflections of a single user's pilot signal from multiple RISs belonging to different operators using neighboring bands. This problem was first identified in [32]. In that work, however, only deterministic channels were considered, and the performance metrics were not applicable to fading channels. In [33], reference [32] was extended to fading channels, and the inter-operator pilot contamination phenomenon was examined through ergodic capacity-based metrics. In [34], inter-operator pilot contamination was studied under discrete phase shifts and various channel conditions. While both [32]

and [33] proposed to orthogonalize the RIS configurations by doubling the number of pilot transmissions to eliminate inter-operator pilot contamination, no practically useful methods were introduced to address this problem to the best of the authors' knowledge. As it will be shown, the design of receive beamforming in the presence of multi-operator RIS is challenging due to the need for aligning with the intended channel and nulling towards the interfering RIS channel, especially when the RIS-BS channels are unstructured.

To address the lack of a practical solution to the inter-operator pilot contamination problem, in this paper, we propose the use of receive beamforming (note that [32] and [33] only considered single-antenna BSs) to eliminate inter-operator pilot contamination. Our scheme allows us to eliminate this phenomenon without doubling the number of pilots to be transmitted.

A. CONTRIBUTIONS

The contributions of this paper can be summarized as follows:

- We propose a BS-based solution to the inter-operator pilot contamination problem that completely eliminates pilot contamination and allows the operators to manage their RISs independently. To the best knowledge of the authors, this is the first beamforming-based solution (and the first solution that does not require an increase in the number of pilots) considered to address pilot contamination in a wireless communication system aided by RISs with multiple operators sharing sites.
- We provide the beamforming vectors necessary for the proposed scheme in closed form in both single- and multi-user cases.
- We compare the proposed scheme with a scheme inspired by [33] where the RISs are jointly configured to be orthogonal, hence eliminating the inter-operator pilot contamination at the expense of doubling the number of transmitted pilots.
- For both the proposed scheme and the alternative scheme based on [33], we provide the MMSE channel estimators and their error covariance matrices in closed form.
- Based on the channel estimators and their covariances, we provide the capacity lower bounds for both schemes under imperfect channel state information (CSI), for which we provide the mean and the variance of the channel conditioned on the channel estimates in closed form.
- We provide numerical examples to compare the performances of the two schemes to demonstrate their advantages and disadvantages.

B. COMPARISON WITH EXISTING PILOT CONTAMINATION MITIGATION SCHEMES

To clarify our contributions further, we provide a comparison between our contributions and references [12]–[15], which all address the pilot contamination problem.

[12] shows that in a multi-cell system with independent Rayleigh fading channels to the BSs, the only limiting factor in system performance is pilot contamination as the number of antennas grows. That is, this phenomenon cannot be avoided by using lots of antennas. [12] also shows that pilot contamination is most severe when the cells operate synchronously. Consequently, the paper concludes that in an asynchronous operation where one cell transmits pilots while the other cells transmit data, the interfering signals would act as uncorrelated noise, which diminishes with infinitely many antennas. In our work, we focus on a single-cell two-operator scenario where pilot transmission occurs synchronously. However, pilot contamination that we consider in this manuscript is not due to multiple UEs transmitting the same pilot but rather multiple RISs use the same sequence of RIS configurations during pilot transmission. Hence, channel uncertainty is created due to the selected pilot scheme, but without causing interference.

In [13], the authors argue that pilot contamination is not the fundamental limit for massive MIMO if the spatial correlation of practical channels is considered. In [13, Theorem 5], it is shown that if a user's spatial correlation matrix is asymptotically linearly independent from its pilot contaminating users' correlation matrices, then the user's SE grows without a bound, i.e., pilot contamination stops being an asymptotically limiting factor. In our manuscript, this corresponds to the asymptotic linear independence of a UE's two channels. Suppose that we consider UE 1. Then, we need to assume that the spatial correlation matrices of the channels UE 1 – RIS 1 and UE 1 – RIS 2 are asymptotically linearly independent, which is quite an optimistic assumption considering that the transmitter of the two channels is the same device and the deployment that we consider is a dense one, where the two RISs are not far apart. That is, we expect that these two channels would have similar spatial correlation matrices and hence it is quite unlikely to have the two matrices linearly independent from each other.

[14] considers a multi-cell setting with interfering users and proposes to address the problem by using a multi-cell MMSE-based precoding, which requires precise orchestration of multiple base stations from different cells. While this approach is effective for inter-cell interference under assuming that there are no synchronization errors across base stations, it is not applicable to a single-cell system. In our system setup, we have two BSs within the same cell belonging to different operators. While Scheme 1 relies on inter-operator RIS coordination, it is not applicable if inter-operator coordination is not present. In contrast, Scheme 2 does not require inter-operator coordination to overcome inter-operator pilot contamination.

[15] considers the inter-cell pilot contamination in a multi-cell setting. By using the coordinated pilot allocation technique, pilot contamination problem is mitigated. In our case, however, this approach is not applicable to the transmitted pilots since pilot contamination comes from the transmitting user itself. That is, self-contamination is the performance-degrading problem. In contrast, the RIS configurations during the channel estimation phase could be coordinated among the operators, which is the essence of one of the pilot contamination mitigation schemes discussed in our manuscript. Table 1 summarizes the discussion in this subsection.

C. ORGANIZATION

We describe the system model in Section II, and formulate the RIS-configuration problem in the multi-operator environment in Section III. Section IV derives the receive beamforming vectors for both Maximum ratio (MR) beamforming and for MR beamforming with null forming towards the interfering channels, when both RIS-BS channels are pure-line of sight (LOS). In Section V, we derive the receive beamforming vectors for unstructured RIS-BS channels based on the Singular Value Decomposition (SVD). In Section VI, we derive the MMSE estimators for both schemes and derive the error covariance matrices in closed form. Based on the analysis in this section, we provide the capacity lower bound under imperfect CSI for both schemes in Section VII, along with the ergodic capacities under perfect CSI. In Section VIII, we demonstrate the extension of the beamforming schemes in Section V to the case of multiple users. We present our numerical results in Section IX and conclude the paper in Section X.

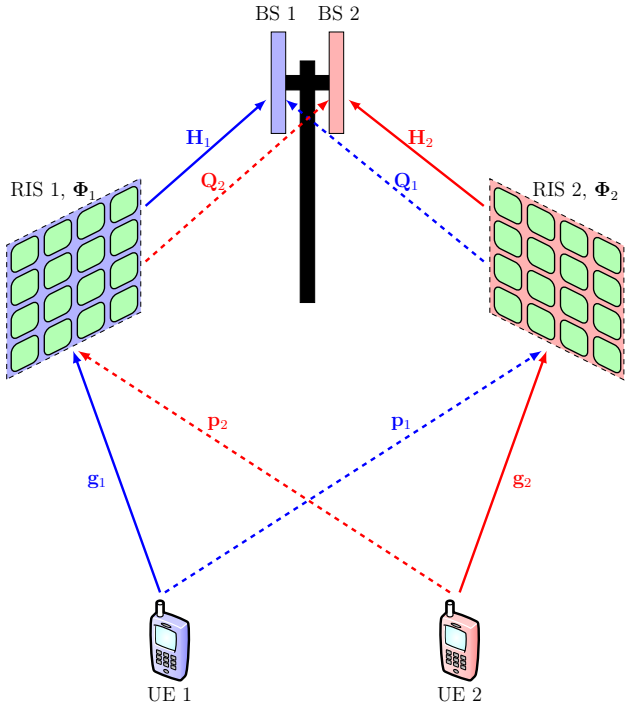

FIGURE 1: The considered setup with two UEs, two RISs, and two co-located M-antenna BSs. The blue channels correspond to frequency band 1, and the red channels correspond to frequency band 2, subscribed by UEs 1 and 2, respectively. The desired channels are denoted by solid lines, while the undesired channels (whose existences might be unknown to the BSs) are denoted by dashed lines. Each channel vector is N-dimensional because each RIS has N elements.

II. SYSTEM MODEL

We consider a single-cell system where two operators share a single site for BS deployment. Each operator employs an M-antenna BS and serves a single user with the help of an N-element RIS. The UEs transmit L pilots over time to explore the different dimensions of the channel. We have devised the system model whose graphical description is provided in Fig. 1 in the light of the practical techno-economical deployment constraints that make it common for multiple MNOs to deploy their BSs on the same tower or rooftop.

The pilot signal $y_{pk}[l] \in \mathbb{C}$ received by the k-th operator's BS at a single time instant l after receive beamforming can be expressed as

$$y_{pk}[l] = \sqrt{P_p}\mathbf{v}_k^T(\mathbf{H}_k\mathbf{\Phi}_k[l]\mathbf{g}_k + \mathbf{Q}_k\mathbf{\Phi}_j[l]\mathbf{p}_k)s_k[l] + \underbrace{\mathbf{v}_k^T\mathbf{n}_k[l]}_{\triangleq w_k[l]}, \tag{1}$$

for $l = 1, \ldots, L$, where $\mathbf{H}_k, \mathbf{Q}_k \in \mathbb{C}^{M\times N}$ denote the channel between RIS k and BS k and the channel between RIS j and BS k, respectively. Although they have the potential to provide additional received signal power, the channels $\mathbf{Q}_k$ for $k = 1, 2$ are considered as interference since the behavior of another operator's RIS cannot be controlled by the operator of interest. We consider a scenario where the gains of the direct links between the BSs and the UEs are negligible compared to the RIS-BS channels and the UE-RIS channels since RISs provide minimal performance gains when the direct link is strong [35, Fig. 4]. Note that since the BSs and the RISs have fixed deployments, it is assumed that both quasi-static RIS-BS channels, $\mathbf{H}_k$ and $\mathbf{Q}_k$, are known by the BSs. As shown in [36], these channels are estimated less frequently compared to the UE-RIS channels. While this assumption holds for static BSs and RISs, this assumption is not applicable to scenarios where the BSs or the RISs are installed on mobile platforms such as unmanned aerial vehicles (UAVs) or high-altitude platform systems (HAPSs) that are on the move. $s_k[l]$ denotes the pilot transmitted by the UE subscribed to the k-th operator at the l-th time instant, and P_p denotes the pilot transmission power. $\mathbf{\Phi}_k[l] = \text{diag}(e^{-j\phi_{k,1}[l]}, \ldots, e^{-j\phi_{k,N}[l]})$ denotes the configuration of the RIS at the l-th time instant belonging to the k-th operator. $\mathbf{n}_k[l] \in \mathbb{C}^{M\times 1} \sim \mathcal{CN}(\mathbf{0}, \sigma_w^2\mathbf{I}_M)$ denotes the noise in the receiver. $\mathbf{v}_k \in \mathbb{C}^{M\times 1}$ denotes the receive beamforming vector employed by the k-th operator with

TABLE 1: Overview of the Existing Pilot Contamination Mitigation Schemes

Reference	Single-cell or Multi-cell	Single Operator or Multiple operator	Traditional or Inter-Operator Pilot Contamination	Key takeaway/Key method to mitigate pilot contamination
Marzetta, [12]	Multi-cell	Single Operator	Traditional	Pilot contamination cannot be mitigated by adding more antennas
Sanguinetti et. al., [13]	Multi-cell	Single Operator	Traditional	Pilot contamination could be mitigated if the tagged user's correlation matrix is asymptotically linearly independent from those of the contaminating users
Jose et al., [14]	Multi-cell	Single Operator	Traditional	Multi-cell MMSE-based precoding
Saxena et al., [15]	Multi-cell	Single Operator	Traditional	Coordinated pilot allocation
This work	Single-cell	Multiple operators	Inter-Operator	Orthogonal RIS configurations/Receive beam & null forming at the base station

$\|\mathbf{v}_k\| = 1$. Note that $w_k[l] = \mathbf{v}_k^T \mathbf{n}_k[l] \sim \mathcal{CN}(0, \sigma_w^2)$ since $\|\mathbf{v}_k\| = 1$. To express (1) in a more compact form, we define $\tilde{\mathbf{h}}_k^T \triangleq \mathbf{v}_k^T \mathbf{H}_k$ and $\tilde{\mathbf{q}}_k^T \triangleq \mathbf{v}_k^T \mathbf{Q}_k$, resulting in

$$y_{pk}[l] = \sqrt{P_p}(\tilde{\mathbf{h}}_k^T \mathbf{\Phi}_k[l]\mathbf{g}_k + \tilde{\mathbf{q}}_k^T \mathbf{\Phi}_j[l]\mathbf{p}_k)s_k[l] + w_k[l]. \quad (2)$$

To obtain a more useful form of (2), we define $\mathbf{D}_{\tilde{\mathbf{h}}_k} = \text{diag}(\tilde{h}_{k1}, \ldots, \tilde{h}_{kN}) \in \mathbb{C}^{N\times N}$, $\mathbf{D}_{\tilde{\mathbf{q}}_k} = \text{diag}(\tilde{q}_{k1}, \ldots, \tilde{q}_{kN}) \in \mathbb{C}^{N\times N}$, $\boldsymbol{\phi}_k[l] = \begin{bmatrix} e^{-j\phi_{k,1}[l]} & \ldots & e^{-j\phi_{k,N}[l]} \end{bmatrix}^T$, and rewrite (2) as

$$y_{pk}[l] = \sqrt{P_p}(\boldsymbol{\phi}_k^T[l]\mathbf{D}_{\tilde{\mathbf{h}}_k}\mathbf{g}_k + \boldsymbol{\phi}_j^T[l]\mathbf{D}_{\tilde{\mathbf{q}}_k}\mathbf{p}_k)s_k[l] + w_k[l], \quad (3)$$

for $l = 1, \ldots, L$. Without loss of generality, we can pick $s_k[l] = 1$ for $l = 1, \ldots, L$, and vertically stack multiple pilot transmissions over time to obtain

$$\mathbf{y}_{pk} = \sqrt{P_p}(\mathbf{B}_k\mathbf{D}_{\tilde{\mathbf{h}}_k}\mathbf{g}_k + \mathbf{B}_j\mathbf{D}_{\tilde{\mathbf{q}}_k}\mathbf{p}_k) + \mathbf{w}_k \in \mathbb{C}^{L\times 1}, \quad (4)$$

where $\mathbf{B}_k = [\boldsymbol{\phi}_1[1], \ldots, \boldsymbol{\phi}_1[L]]^T \in \mathbb{C}^{L\times N}$ denotes the vertically stacked RIS configurations over time. It has to be noted that (4) is very similar to [33, Eq. 3], where the problem of inter-operator pilot contamination is introduced. In [33], however, this problem was treated in a single-antenna BS setting and was mitigated by choosing orthogonal RIS configurations at the cost of doubling the pilot transmission overhead. In this manuscript, we look into how receive beamforming at a multi-antenna BS can be used to address this problem. In the next section, we formulate the channel estimation problem and demonstrate how the use of multiple RISs by different operators causes inter-operator pilot contamination.

III. PROBLEM FORMULATION

Based on (4), operator k aims to estimate $\mathbf{g}_k \sim \mathcal{CN}(\mathbf{0}, \mathbf{\Sigma}_{\mathbf{g}_k})$ and $\mathbf{p}_k \sim \mathcal{CN}(\mathbf{0}, \mathbf{\Sigma}_{\mathbf{p}_k})$. To this end, the BS employs the MMSE estimator. To express the estimator in a compact form, we define the following covariance matrices:

$$\mathbf{C}_{\mathbf{gy}} = \mathbb{E}[\mathbf{g}_k\mathbf{y}_{pk}^H] \in \mathbb{C}^{N\times L}, \quad (5a)$$
$$\mathbf{C}_{\mathbf{py}} = \mathbb{E}[\mathbf{p}_k\mathbf{y}_{pk}^H] \in \mathbb{C}^{N\times L}, \quad (5b)$$
$$\mathbf{C}_{\mathbf{yy}} = \mathbb{E}[\mathbf{y}_{pk}\mathbf{y}_{pk}^H] \in \mathbb{C}^{L\times L}. \quad (5c)$$

As a result, the MMSE estimators for $\mathbf{g}_k$ and $\mathbf{p}_k$ become

$$\hat{\mathbf{g}}_k = \mathbf{C}_{\mathbf{gy}}\mathbf{C}_{\mathbf{yy}}^{-1}\mathbf{y}_{pk}, \quad (6a)$$
$$\hat{\mathbf{p}}_k = \mathbf{C}_{\mathbf{py}}\mathbf{C}_{\mathbf{yy}}^{-1}\mathbf{y}_{pk}. \quad (6b)$$

The resulting error covariances can be expressed as

$$\mathbf{\Sigma}_{\mathbf{e}_{\mathbf{g}_k}} = \mathbb{E}[(\mathbf{g}_k - \hat{\mathbf{g}}_k)(\mathbf{g}_k - \hat{\mathbf{g}}_k)^H] = \mathbf{\Sigma}_{\mathbf{g}_k} - \mathbf{C}_{\mathbf{gy}}\mathbf{C}_{\mathbf{yy}}^{-1}\mathbf{C}_{\mathbf{gy}}^H, \quad (7a)$$

$$\mathbf{\Sigma}_{\mathbf{e}_{\mathbf{p}_k}} = \mathbb{E}[(\mathbf{p}_k - \hat{\mathbf{p}}_k)(\mathbf{p}_k - \hat{\mathbf{p}}_k)^H] = \mathbf{\Sigma}_{\mathbf{p}_k} - \mathbf{C}_{\mathbf{py}}\mathbf{C}_{\mathbf{yy}}^{-1}\mathbf{C}_{\mathbf{py}}^H. \quad (7b)$$

Note that in the absence of pilot contamination, the covariance matrices of $\hat{\mathbf{g}}_k$ and $\hat{\mathbf{p}}_k$ approach to $\mathbf{\Sigma}_{\mathbf{g}_k}$ and $\mathbf{\Sigma}_{\mathbf{p}_k}$ as

$P_p \to \infty$. Consequently, $\mathbf{\Sigma}_{\mathbf{e}_{\mathbf{g}_k}}$ and $\mathbf{\Sigma}_{\mathbf{e}_{\mathbf{p}_k}}$ approach to $\mathbf{0}$ as $P_p \to \infty$, so the estimation will be error-free.

As shown in [33], inter-operator pilot contamination arises when $\mathbf{B}_1^H \mathbf{B}_2 \neq \mathbf{0}$. In this section, we will consider the special case $\mathbf{B}_1 = \mathbf{B}_2 = \mathbf{B}$ for demonstration purposes. As a result, we can explicitly express the covariance matrices we defined in (5) as

$$\mathbf{C}_{\mathbf{gy}} = \sqrt{P_p}\mathbf{\Sigma}_{\mathbf{g}_k}\mathbf{D}_{\tilde{\mathbf{h}}_k}^H \mathbf{B}^H, \tag{8a}$$

$$\mathbf{C}_{\mathbf{py}} = \sqrt{P_p}\mathbf{\Sigma}_{\mathbf{p}_k}\mathbf{D}_{\tilde{\mathbf{q}}_k}^H \mathbf{B}^H, \tag{8b}$$

$$\mathbf{C}_{\mathbf{yy}} = P_p \mathbf{B}(\mathbf{D}_{\tilde{\mathbf{h}}_k}\mathbf{\Sigma}_{\mathbf{g}_k}\mathbf{D}_{\tilde{\mathbf{h}}_k}^H + \mathbf{D}_{\tilde{\mathbf{q}}_k}\mathbf{\Sigma}_{\mathbf{p}_k}\mathbf{D}_{\tilde{\mathbf{q}}_k}^H)\mathbf{B}^H + \sigma_w^2 \mathbf{I}_L. \tag{8c}$$

The $\mathbf{B}$ and $\mathbf{B}^H$ terms can be inserted inside the inversion using their pseudoinverses. As a result, the estimator covariances in explicit form can be expressed as

$$\mathbf{\Sigma}_{\hat{\mathbf{g}}_k} = \mathbf{\Sigma}_{\mathbf{g}_k}\mathbf{D}_{\tilde{\mathbf{h}}_k}^H \Big(\mathbf{D}_{\tilde{\mathbf{h}}_k}\mathbf{\Sigma}_{\mathbf{g}_k}\mathbf{D}_{\tilde{\mathbf{h}}_k}^H + \mathbf{D}_{\tilde{\mathbf{q}}_k}\mathbf{\Sigma}_{\mathbf{p}_k}\mathbf{D}_{\tilde{\mathbf{q}}_k}^H + \frac{\sigma_w^2}{P_p}\mathbf{I}_L\Big)^{-1} \times \mathbf{D}_{\tilde{\mathbf{h}}_k}\mathbf{\Sigma}_{\mathbf{g}_k}, \tag{9a}$$

$$\mathbf{\Sigma}_{\hat{\mathbf{p}}_k} = \mathbf{\Sigma}_{\mathbf{p}_k}\mathbf{D}_{\tilde{\mathbf{q}}_k}^H \Big(\mathbf{D}_{\tilde{\mathbf{h}}_k}\mathbf{\Sigma}_{\mathbf{g}_k}\mathbf{D}_{\tilde{\mathbf{h}}_k}^H + \mathbf{D}_{\tilde{\mathbf{q}}_k}\mathbf{\Sigma}_{\mathbf{p}_k}\mathbf{D}_{\tilde{\mathbf{q}}_k}^H + \frac{\sigma_w^2}{P_p}\mathbf{I}_L\Big)^{-1} \times \mathbf{D}_{\tilde{\mathbf{q}}_k}\mathbf{\Sigma}_{\mathbf{p}_k}. \tag{9b}$$

If we take the limit as $P_p \to \infty$, we obtain

$$\mathbf{\Sigma}_{\hat{\mathbf{g}}_k} = \mathbf{\Sigma}_{\mathbf{g}_k}\mathbf{D}_{\tilde{\mathbf{h}}_k}^H \Big(\mathbf{D}_{\tilde{\mathbf{h}}_k}\mathbf{\Sigma}_{\mathbf{g}_k}\mathbf{D}_{\tilde{\mathbf{h}}_k}^H + \mathbf{D}_{\tilde{\mathbf{q}}_k}\mathbf{\Sigma}_{\mathbf{p}_k}\mathbf{D}_{\tilde{\mathbf{q}}_k}^H\Big)^{-1}\mathbf{D}_{\tilde{\mathbf{h}}_k}\mathbf{\Sigma}_{\mathbf{g}_k}, \tag{10a}$$

$$\mathbf{\Sigma}_{\hat{\mathbf{p}}_k} = \mathbf{\Sigma}_{\mathbf{p}_k}\mathbf{D}_{\tilde{\mathbf{q}}_k}^H \Big(\mathbf{D}_{\tilde{\mathbf{h}}_k}\mathbf{\Sigma}_{\mathbf{g}_k}\mathbf{D}_{\tilde{\mathbf{h}}_k}^H + \mathbf{D}_{\tilde{\mathbf{q}}_k}\mathbf{\Sigma}_{\mathbf{p}_k}\mathbf{D}_{\tilde{\mathbf{q}}_k}^H\Big)^{-1}\mathbf{D}_{\tilde{\mathbf{q}}_k}\mathbf{\Sigma}_{\mathbf{p}_k}. \tag{10b}$$

Note that in both cases, the estimator covariances fail to approach the parameter covariances due to inter-operator pilot contamination. That is, $\lim_{P_p\to\infty}\mathbf{\Sigma}_{\hat{\mathbf{g}}_k} \neq \mathbf{\Sigma}_{\mathbf{g}_k}$ and $\lim_{P_p\to\infty}\mathbf{\Sigma}_{\hat{\mathbf{p}}_k} \neq \mathbf{\Sigma}_{\mathbf{p}_k}$. To overcome this, we either have to pick $\mathbf{B}_1^H\mathbf{B}_2 = \mathbf{0}$ so that both covariances converge to their parameter covariances or we have to pick $\mathbf{v}_k$ such that one of $\tilde{\mathbf{h}}_k$ and $\tilde{\mathbf{q}}_k$ become $\mathbf{0}$. Nulling the latter is preferable as $\tilde{\mathbf{h}}_k$ goes through the operator's own RIS, whose configuration is controllable. In Sections IV and V, we look into the problem of designing $\mathbf{v}_k$ depending on the structures of $\mathbf{H}_k$ and $\mathbf{Q}_k$. Then, in Section VI, we will provide the asymptotic analysis of the estimators' behavior when pilot contamination is eliminated.

IV. RECEIVE BEAMFORMING FOR PURE-LOS RIS-BS CHANNELS

In this section, we look into how receive beamforming can be utilized to overcome inter-operator pilot contamination when both $\mathbf{H}_k$ and $\mathbf{Q}_k$ exhibit a pure LOS structure. We denote the angle of departure (AoD) and angle of arrival (AoA) for $\mathbf{H}_k$ and $\mathbf{Q}_k$ as $\theta_{\mathbf{H}_k}^{\text{AoD}}$, $\theta_{\mathbf{H}_k}^{\text{AoA}}$, $\theta_{\mathbf{Q}_k}^{\text{AoD}}$, and $\theta_{\mathbf{Q}_k}^{\text{AoA}}$, respectively. In addition, we denote the array steering vectors for the k-th BSs and RISs as $\mathbf{a}_k^{\text{BS}}(\cdot) : \mathbb{R} \mapsto \mathbb{C}^{M\times 1}$ and $\mathbf{a}_k^{\text{RIS}}(\cdot) : \left[-\frac{\pi}{2}, \frac{\pi}{2}\right] \times [0, +\infty) \mapsto \mathbb{C}^{N\times 1}$. Then, we can express $\mathbf{H}_k$ and $\mathbf{Q}_k$ as

$$\mathbf{H}_k = \sqrt{\alpha_{\mathbf{H}_k}} e^{-j\beta_{\mathbf{H}_k}} \mathbf{a}_k^{\text{BS}}(\theta_{\mathbf{H}_k}^{\text{AoA}}, \lambda_k)\mathbf{a}_k^{\text{RIS}\,H}(\theta_{\mathbf{H}_k}^{\text{AoD}}, \lambda_k), \tag{11a}$$

$$\mathbf{Q}_k = \sqrt{\alpha_{\mathbf{Q}_k}} e^{-j\beta_{\mathbf{Q}_k}} \mathbf{a}_k^{\text{BS}}(\theta_{\mathbf{Q}_k}^{\text{AoA}}, \lambda_k)\mathbf{a}_j^{\text{RIS}\,H}(\theta_{\mathbf{Q}_k}^{\text{AoD}}, \lambda_k), \tag{11b}$$

where $\alpha_{\mathbf{H}_k}$ and $\alpha_{\mathbf{Q}_k}$ denote the path loss coefficients for the channels $\mathbf{H}_k$ and $\mathbf{Q}_k$, respectively, and $\beta_{\mathbf{H}_k}$ and $\beta_{\mathbf{Q}_k}$ denote the phase shifts caused by the propagation delays over the channels $\mathbf{H}_k$ and $\mathbf{Q}_k$, respectively. For simplicity, we consider uniform linear array (ULA) structures for all BSs and RISs, however, it has to be noted that the analysis in this section can be extended to any array geometry.* Hence, we can express the steering vectors in (11) as

$$\mathbf{a}_k^{\text{BS}}(\theta, \lambda) = \begin{bmatrix} 1 & e^{-j2\pi\frac{d_k}{\lambda}\sin\theta} & \dots & e^{-j2\pi\frac{d_k}{\lambda}(M-1)\sin\theta} \end{bmatrix}^T, \tag{12a}$$

$$\mathbf{a}_k^{\text{RIS}}(\theta, \lambda) = \begin{bmatrix} 1 & e^{-j2\pi\frac{d_k}{\lambda}\sin\theta} & \dots & e^{-j2\pi\frac{d_k}{\lambda}(N-1)\sin\theta} \end{bmatrix}^T, \tag{12b}$$

where d_k denotes the inter-element spacing used by the k-th operator and θ is angle measured from the broadside direction.

A. ALIGNING THE BEAM WITH THE INTENDED CHANNEL

Among the RIS-BS channels, note that $\mathbf{H}_k$ is the intended channel for reception. In contrast, $\mathbf{Q}_k$ is the interfering channel causing the inter-operator pilot contamination as it is the link between the intended operator's BS and the other operator's RIS. This channel is considered as interference as it involves a RIS that is not controllable by the operator of interest. To align with the intended channel, the following receive beamforming vector must be used:

$$\mathbf{v}_{k,A}^T = \frac{1}{\sqrt{M}}\mathbf{a}_k^{\text{BS}\,H}\left(\theta_{\mathbf{H}_k}^{\text{AoA}}, \lambda_k\right). \tag{13}$$

As a result, the following equivalent multiple-input single-output (MISO) channels arise:

$$\tilde{\mathbf{h}}_k = \sqrt{M\alpha_{\mathbf{H}_k}} e^{-j\beta_{\mathbf{H}_k}} \mathbf{a}_k^{\text{RIS}\,*}\left(\theta_{\mathbf{H}_k}^{\text{AoD}}, \lambda_k\right), \tag{14a}$$

$$\tilde{\mathbf{q}}_k = \sqrt{\frac{\alpha_{\mathbf{Q}_k}}{M}} e^{-j\beta_{\mathbf{Q}_k}} \underbrace{\mathbf{a}_k^{\text{BS}\,H}(\theta_{\mathbf{H}_k}^{\text{AoA}}, \lambda_k)\mathbf{a}_k^{\text{BS}}\left(\theta_{\mathbf{Q}_k}^{\text{AoA}}, \lambda_k\right)}_{\triangleq \eta_k} \times \mathbf{a}_j^{\text{RIS}\,*}(\theta_{\mathbf{Q}_k}^{\text{AoD}}, \lambda_k). \tag{14b}$$

This beamforming vector aligns the BS's reception with $\mathbf{H}_k$. However, some interference will remain from $\mathbf{Q}_k$ as there is no null forming in that direction; that is, η_k will be non-zero. In the next subsection, we propose a method to remove this residual interference.

*This can be done by considering the relevant array steering vector and applying the formulae accordingly.

TABLE 2: Summary of correlations between AoA steering vectors and the two beamforming vectors where $\mathbf{v}_{k,A}$ is the beamforming vector maximizing the gain from the intended channel, and $\mathbf{v}_{k,B}$ is the beamforming vector resulting from placing nulls into the first beamformer.

	$\mathbf{a}_k^{\text{BS}}(\theta_{\mathbf{H}_k}^{\text{AoA}})$	$\mathbf{a}_k^{\text{BS}}(\theta_{\mathbf{Q}_k}^{\text{AoA}})$
$\mathbf{v}_{k,A}^T$	$\sqrt{M}$	η_k
$\mathbf{v}_{k,B}^T$	$\sqrt{M-\frac{\lvert\eta_k\rvert^2}{M}}$	0

B. ALIGNING THE BEAM WITH THE INTENDED CHANNEL WHILE NULLING THE INTERFERING CHANNEL

To combat the problem of residual interference, we can choose the receive combining to place a null towards $\mathbf{Q}_k$ by using orthogonal projection. We can first beamform towards $\mathbf{H}_k$, then subtract the correlated component to $\mathbf{Q}_k$. We can achieve this through the Gram-Schmidt orthogonalization process, which can be expressed as follows:

$$\tilde{\mathbf{v}}_{k,B}^T = \mathbf{a}_k^{\text{BS}\,H}(\theta_{\mathbf{H}_k}^{\text{AoA}},\lambda_k) - \eta_k \frac{\mathbf{a}_k^{\text{BS}\,H}(\theta_{\mathbf{Q}_k}^{\text{AoA}},\lambda_k)}{\|\mathbf{a}_k^{\text{BS}}(\theta_{\mathbf{Q}_k}^{\text{AoA}},\lambda_k)\|^2}. \tag{15}$$

Note that the resulting beamforming vector in (15) will have a different l_2 norm than 1. To normalize it, we need to multiply it with $\frac{1}{\|\tilde{\mathbf{v}}_{k,B}^T\|}$, which results in

$$\mathbf{v}_{k,B}^T = \frac{1}{\|\tilde{\mathbf{v}}_{k,B}^T\|}\tilde{\mathbf{v}}_{k,B}^T, \tag{16}$$

where $\|\tilde{\mathbf{v}}_{k,B}\|^2 = M - \frac{|\eta_k|^2}{M}$. To express (14) for $\mathbf{v}_{k,B}^T$, we need to compute $\mathbf{v}_{k,B}^T\mathbf{a}_k^{\text{BS}}(\theta_{\mathbf{H}_k}^{\text{AoA}})$ and $\mathbf{v}_{k,B}^T\mathbf{a}_k^{\text{BS}}(\theta_{\mathbf{Q}_k}^{\text{AoA}})$. These can be expressed as follows:

$$\mathbf{v}_{k,B}^T\mathbf{a}_k^{\text{BS}}(\theta_{\mathbf{H}_k}^{\text{AoA}}) = \sqrt{M-\frac{|\eta_k|^2}{M}}, \tag{17a}$$

$$\mathbf{v}_{k,B}^T\mathbf{a}_k^{\text{BS}}(\theta_{\mathbf{Q}_k}^{\text{AoA}}) = \sqrt{\frac{1}{M-\frac{|\eta_k|^2}{M}}}(\eta_k-\eta_k) = 0. \tag{17b}$$

Note that $\mathbf{v}_{k,B}^T$ completely eliminates the interference coming from $\mathbf{Q}_k$ and hence the inter-operator pilot contamination. On the other hand, the gain from $\mathbf{H}_k$ is multiplied by a factor of $\sqrt{1-\frac{|\eta_k|^2}{M^2}} \in [0,1]$. This factor takes the value 0 when $|\eta_k| = M$ and 1 when $\eta_k = 0$. This implies that when the receiver steering vectors of $\mathbf{H}_k$ and $\mathbf{Q}_k$ are orthogonal, there is no loss in the gain from $\mathbf{H}_k$, and $\mathbf{v}_{k,A}$ and $\mathbf{v}_{k,B}$ are equivalent. On the other hand, if $|\eta_k| = M$ and hence the receive steering vectors are fully correlated, then $\mathbf{v}_{k,B}$ nullforms towards both channels and $\mathbf{v}_{k,A}$ beamforms towards both channels. The former case is the best-case scenario, while the latter is the worst-case scenario, i.e., when inter-operator pilot contamination cannot be eliminated. A summary of the resulting correlations can be found in Table 2. As a result, we can express the effective MISO channels as follows:

$$\tilde{\mathbf{h}}_k = \sqrt{M-\frac{|\eta_k|^2}{M}}\sqrt{\alpha_{\mathbf{H}_k}}e^{-j\beta_{\mathbf{H}_k}}\mathbf{a}_k^{\text{RIS}}(\theta_{\mathbf{H}_k}^{\text{AoD}},\lambda_k), \tag{18a}$$

$$\tilde{\mathbf{q}}_k = \mathbf{0}. \tag{18b}$$

Note that for pure-LOS RIS-BS channels, we can explicitly use the direction of arrival (DoA) information to construct the receive beamforming vector. However, it is not always possible to keep track of all reflections in the environment spatially in the presence of multiple dominant paths. To this end, a more generic approach has to be taken. To this end, the structural assumptions on the channels have to be replaced with a more generic approach and SVD analysis has to be formed. We demonstrate this in the next section.

V. RECEIVE BEAMFORMING FOR UNSTRUCTURED RIS-BS CHANNELS

In this section, we look into how receive beamforming can be utilized to overcome inter-operator pilot contamination when neither $\mathbf{H}_k$ nor $\mathbf{Q}_k$ exhibits any particular structure. Unstructured MIMO channels can be expressed as a weighted sum of rank-1 matrices, which can be done by SVD. The singular values are the weights of the rank-1 matrices, and the left and right singular vectors correspond to the vectors forming the outer product. That is, for the SVD

$$\mathbf{A} = \mathbf{U}\mathbf{\Sigma}\mathbf{V}^H \in \mathbb{C}^{M\times N}, \tag{19}$$

we have that $\mathbf{A} = \sum_{k=1}^{N}\sigma_k\mathbf{u}_k\mathbf{v}_k^H$. We already know how to treat rank-1 channels for beamforming purposes from Section IV. To apply the same principles, we need to identify the dominant rank-1 channel within $\mathbf{H}_k$, and the non-zero rank-1 components of $\mathbf{Q}_k$, for which we need to take their SVDs. Suppose that $\mathbf{H}_k$ and $\mathbf{Q}_k$ have the following SVDs:

$$\mathbf{H}_k = \mathbf{\Gamma}_k\mathbf{\Sigma}_k\mathbf{\Upsilon}_k^H, \tag{20a}$$

$$\mathbf{Q}_k = \mathbf{\Delta}_k\mathbf{\Xi}_k\mathbf{\Omega}_k^H. \tag{20b}$$

We denote the singular vectors as $\mathbf{\Gamma}_k = \begin{bmatrix}\boldsymbol{\gamma}_{k,1} & \dots & \boldsymbol{\gamma}_{k,M}\end{bmatrix} \in \mathbb{C}^{M\times M}$, $\mathbf{\Delta}_k = \begin{bmatrix}\boldsymbol{\delta}_{k,1} & \dots & \boldsymbol{\delta}_{k,M}\end{bmatrix} \in \mathbb{C}^{M\times M}$, $\mathbf{\Upsilon}_k = \begin{bmatrix}\boldsymbol{\upsilon}_{k,1} & \dots & \boldsymbol{\upsilon}_{k,N}\end{bmatrix} \in \mathbb{C}^{N\times N}$, and $\mathbf{\Omega}_k = \begin{bmatrix}\boldsymbol{\omega}_{k,1} & \dots & \boldsymbol{\omega}_{k,N}\end{bmatrix} \in \mathbb{C}^{N\times N}$. Denote the singular values of $\mathbf{H}$ as $\sigma_1,\dots,\sigma_N$ and those of $\mathbf{Q}$ as $\xi_1,\dots,\xi_N$.

A. ALIGNING THE BEAM WITH THE INTENDED CHANNEL

To align our reception with $\mathbf{H}_k$ using a vector $\mathbf{v}_k$, we need to align $\mathbf{v}_k$ with the left singular vector of $\mathbf{H}_k$ corresponding to the largest singular value. Let us denote this singular vector as $\boldsymbol{\gamma}_{k,C}$. Then, we set $\mathbf{v}_k$ as

$$\mathbf{v}_{k,C}^T = \boldsymbol{\gamma}_{k,C}^H. \tag{21}$$

Based on this selection of the beamforming vector, the effective MISO channels become

$$\tilde{\mathbf{h}}_k^T = \sigma_{k,C}\boldsymbol{\upsilon}_{k,C}^H, \tag{22a}$$

$$\tilde{\mathbf{q}}_k^T = \boldsymbol{\gamma}_{k,C}^H\mathbf{Q}_k, \tag{22b}$$

where $\sigma_{k,C}$ is the largest singular value of $\mathbf{H}_k$ and $\boldsymbol{\upsilon}_{k,C}$ is the corresponding right singular vector.

B. ALIGNING THE BEAM WITH THE INTENDED CHANNEL WHILE NULLING THE INTERFERING CHANNEL

While beamforming according to the largest singular value of the intended channel $\mathbf{H}_k$ yields the maximum gain possible, it has to be noted that this scheme does not remove the interference coming from $\mathbf{Q}_k$, which causes the inter-operator pilot contamination. However, this interference has to be removed to obtain reliable channel estimates. To this end, we consider removing the components correlated to the singular vectors of $\mathbf{Q}_k$ corresponding to non-zero singular values. We can assume that $\mathbf{Q}_k$ has $R < \min(M, N)$ non-zero singular values since for the scenarios where RISs are actually useful, RIS-BS channels tend to be LOS-dominant, albeit not necessarily pure-LOS. Such scenarios tend to result in rank-deficient (or high-condition number) channel matrices. The following method to orthogonalize $\mathbf{v}_k$ to $\boldsymbol{\delta}_{k,1}, \ldots, \boldsymbol{\delta}_{k,R}$ requires that $R < M$, which is already satisfied for $M \geq N$ but not always the case when $N > M$. We can utilize the Gram-Schmidt process to orthogonalize the beamforming vector to all singular vectors of $\mathbf{Q}_k$ corresponding to non-zero singular values. This process can be expressed as follows:

$$\begin{aligned}
\tilde{\mathbf{v}}_{k,D}^{(0)^T} &= \boldsymbol{\gamma}_{k,C}^H, \\
\tilde{\mathbf{v}}_{k,D}^{(1)^T} &= \tilde{\mathbf{v}}_{k,D}^{(0)^T} - \frac{\boldsymbol{\delta}_{k,1}^H \tilde{\mathbf{v}}_{k,D}^{(0)}}{\|\boldsymbol{\delta}_{k,1}\|^2} \boldsymbol{\delta}_{k,1}^H, \\
\tilde{\mathbf{v}}_{k,D}^{(2)^T} &= \tilde{\mathbf{v}}_{k,D}^{(1)^T} - \frac{\boldsymbol{\delta}_{k,2}^H \tilde{\mathbf{v}}_{k,D}^{(1)}}{\|\boldsymbol{\delta}_{k,2}\|^2} \boldsymbol{\delta}_{k,2}^H, \\
&\vdots \\
\tilde{\mathbf{v}}_{k,D}^{(R)^T} &= \tilde{\mathbf{v}}_{k,D}^{(R-1)^T} - \frac{\boldsymbol{\delta}_{k,R}^H \tilde{\mathbf{v}}_{k,D}^{(R-1)}}{\|\boldsymbol{\delta}_{k,R}\|^2} \boldsymbol{\delta}_{k,R}^H. \qquad (23)
\end{aligned}$$

Next, we normalize (23) to obtain the beamforming vector towards $\mathbf{H}_k$ that also nullforms towards $\mathbf{Q}_k$ as

$$\mathbf{v}_{k,D} = \frac{1}{\|\tilde{\mathbf{v}}_{k,D}\|} \tilde{\mathbf{v}}_{k,D}^{(R)}. \qquad (24)$$

Remark: The described process is equivalent to projecting the beamforming vector onto the nullspace of $\mathbf{Q}_k$.

VI. CHANNEL ESTIMATION BASED ON CORRELATED RAYLEIGH FADING PRIORS

Since $\mathbf{H}_k$ and $\mathbf{Q}_k$ are already known at the BS, the BS aims to estimate $\mathbf{g}_k$ and $\mathbf{p}_k$ for $k = 1, 2$. Since the beamforming vectors $\mathbf{v}_k$ are also known by the BSs, the effective RIS-BS MISO channels $\tilde{\mathbf{h}}_k$ and $\tilde{\mathbf{q}}_k$ are also known. Sections IV and V focus on shaping the channels $\tilde{\mathbf{h}}_k$ and $\tilde{\mathbf{q}}_k$ using receive beamforming. Specifically, when null forming towards $\mathbf{Q}_k$ is applied, the effect of the unintended path through the other operator's RIS is essentially removed. In [33, Sec. V], a detailed analysis of the channel estimation covariances for a model equivalent to (4) is provided. To investigate the impact of RIS configurations on inter-operator pilot contamination, in this paper, we consider three scenarios:

1) The user transmits $L = 2N$ pilots. The operators configure their RISs such that $\mathbf{B}_1^H \mathbf{B}_2 = \mathbf{0}$, and both operators beamform towards $\mathbf{H}_k$'s without null forming towards $\mathbf{Q}_k$'s. For conciseness, we will call this *Scheme 1*.
2) The user transmits $L = N$ pilots. The operators configure their RISs such that $\mathbf{B}_1 = \mathbf{B}_2$, and both operators beamform towards $\mathbf{H}_k$'s and nullform towards $\mathbf{Q}_k$'s. For conciseness, we will call this *Scheme 2*.
3) In the baseline scheme, the user transmits $L = N$ pilots. The operators configure their RISs such that $\mathbf{B}_1 = \mathbf{B}_2$, and both operators beamform towards $\mathbf{H}_k$'s without null forming towards $\mathbf{Q}_k$'s. For conciseness, we will call this *the baseline scheme*.

Note that in scheme 1 and the baseline scheme, both $\mathbf{g}_k$ and $\mathbf{p}_k$ are to be estimated, hence at least $2N$ pilots are required. In scheme 2, only $\mathbf{g}_k$ is estimated since nulling $\mathbf{Q}_k$ removes the necessity of estimating $\mathbf{p}_k$, hence at least N pilots are required. For each scenario, we provide the resulting channel estimation error covariances to evaluate the data communication performance under imperfect CSI later on.

A. SCHEME 1

In this scheme, the receive beamforming captures the maximum energy from the intended channel, but it does not suppress interference. However, the interference is canceled by separating RIS configuration sequences, which is enabled by doubling the number of transmitted pilots and picking $\mathbf{B}_1^H \mathbf{B}_2 = \mathbf{0}$. Consequently, using this scheme, the following received pilot signal models arise:

$$\mathbf{y}_{p1} = \sqrt{P_p}(\mathbf{B}_1 \mathbf{D}_{\tilde{\mathbf{h}}_1} \mathbf{g}_1 + \mathbf{B}_2 \mathbf{D}_{\tilde{\mathbf{q}}_1} \mathbf{p}_1) + \mathbf{w}_1 \in \mathbb{C}^{L \times 1}, \qquad (25a)$$

$$\mathbf{y}_{p2} = \sqrt{P_p}(\mathbf{B}_2 \mathbf{D}_{\tilde{\mathbf{h}}_2} \mathbf{g}_2 + \mathbf{B}_1 \mathbf{D}_{\tilde{\mathbf{q}}_2} \mathbf{p}_2) + \mathbf{w}_2 \in \mathbb{C}^{L \times 1}. \qquad (25b)$$

To design $\mathbf{B}_1$ and $\mathbf{B}_2$ such that $\mathbf{B}_1^H \mathbf{B}_2 = \mathbf{0}$, we need $2N$-many L-dimensional vectors that are orthogonal to each other. Hence, the operators need to transmit $L \geq 2N$ many pilots.

B. SCHEME 2

In this scheme, the receive beamforming captures the maximum energy from the intended channel while suppressing the interference from $\mathbf{Q}_k$. This interference suppression by null forming causes the beamformer to capture less energy from $\mathbf{H}_k$. On the other hand, it is no longer necessary to orthogonalize the sequences of RIS configurations – and hence to double the number of transmitted pilots – since inter-operator pilot contamination is removed by receive beamforming. Therefore, this scheme configures the RISs without orthogonalizing them to each other, that is, $\mathbf{B}_1 = \mathbf{B}_2$. This approach uses half as many pilot transmissions as Scheme 1. Consequently, the following received pilot signal

models arise:

$$\mathbf{y}_{p1} = \sqrt{P_p}\mathbf{B}_1\mathbf{D}_{\tilde{\mathbf{h}}_1}\mathbf{g}_1 + \mathbf{w}_1 \in \mathbb{C}^{L\times 1}, \tag{26a}$$

$$\mathbf{y}_{p2} = \sqrt{P_p}\mathbf{B}_2\mathbf{D}_{\tilde{\mathbf{h}}_2}\mathbf{g}_2 + \mathbf{w}_2 \in \mathbb{C}^{L\times 1}, \tag{26b}$$

In this scheme, the operators do not have the requirement $\mathbf{B}_1^H\mathbf{B}_2 = \mathbf{0}$, hence L could be less than $2N$. However, $L \geq N$ is still a requirement since the operators need at least as many observations as the number of unknown parameters.

C. BASELINE SCHEME

In this scheme, the receive beamforming is done as in Scheme 1. Unlike Scheme 1, however, the interference is not canceled by orthogonalizing the RISs, and $\mathbf{B}_1 = \mathbf{B}_2$ is adopted as in Scheme 2, but without null forming. Consequently, the following received pilot signal models arise:

$$\mathbf{y}_{p1} = \sqrt{P_p}(\mathbf{B}_1\mathbf{D}_{\tilde{\mathbf{h}}_1}\mathbf{g}_1 + \mathbf{B}_2\mathbf{D}_{\tilde{\mathbf{q}}_1}\mathbf{p}_1) + \mathbf{w}_1 \in \mathbb{C}^{L\times 1}, \tag{27a}$$

$$\mathbf{y}_{p2} = \sqrt{P_p}(\mathbf{B}_2\mathbf{D}_{\tilde{\mathbf{h}}_2}\mathbf{g}_2 + \mathbf{B}_1\mathbf{D}_{\tilde{\mathbf{q}}_2}\mathbf{p}_2) + \mathbf{w}_2 \in \mathbb{C}^{L\times 1}, \tag{27b}$$

The same principles apply for this scheme as Scheme 2, hence, we have that $L \geq N$.

D. IMPACT OF THE CHOICE OF SCHEME ON MMSE CHANNEL ESTIMATION PERFORMANCE

In Section III, we have demonstrated the channel estimation mean squared errors (MSEs). The discussion so far impacts the MSE by the following means:

- The choice of scheme affects $\mathbf{C}_{\mathbf{yy}}$ as the path over the other operator's RIS is nulled when nullforming is applied.
- The gains of $\tilde{\mathbf{h}}_k$ and $\tilde{\mathbf{q}}_k$ are affected by how beamforming is carried out. Since both Scheme 1 and scheme 2 null the unintended path over the other operator's RIS, (9) becomes

$$\mathbf{\Sigma}_{\hat{\mathbf{g}}_k} = \mathbf{\Sigma}_{\mathbf{g}_k}\mathbf{D}_{\tilde{\mathbf{h}}_k}^H\left(\mathbf{D}_{\tilde{\mathbf{h}}_k}\mathbf{\Sigma}_{\mathbf{g}_k}\mathbf{D}_{\tilde{\mathbf{h}}_k}^H + \frac{\sigma_w^2}{P_p}\mathbf{I}_L\right)^{-1}\mathbf{D}_{\tilde{\mathbf{h}}_k}\mathbf{\Sigma}_{\mathbf{g}_k}, \tag{28a}$$

$$\mathbf{\Sigma}_{\hat{\mathbf{p}}_k} = \mathbf{\Sigma}_{\mathbf{p}_k}\mathbf{D}_{\tilde{\mathbf{q}}_k}^H\left(\mathbf{D}_{\tilde{\mathbf{q}}_k}\mathbf{\Sigma}_{\mathbf{p}_k}\mathbf{D}_{\tilde{\mathbf{q}}_k}^H + \frac{\sigma_w^2}{P_p}\mathbf{I}_L\right)^{-1}\mathbf{D}_{\tilde{\mathbf{q}}_k}\mathbf{\Sigma}_{\mathbf{p}_k} \tag{28b}$$

Consequently, the result of (7) changes depending on which scheme is adopted. Next, we consider the asymptotic behavior of the covariances of the estimators for Scheme 1 and the baseline scheme to examine the impact of inter-operator pilot contamination.

E. ASYMPTOTIC BEHAVIOR OF ESTIMATOR COVARIANCES

For all schemes, the estimator covariances can be expressed as

$$\mathbf{\Sigma}_{\hat{\mathbf{g}}_k} = \mathbf{C}_{\mathbf{gy}}\mathbf{C}_{\mathbf{yy}}^{-1}\mathbf{C}_{\mathbf{gy}}^H, \tag{29a}$$

$$\mathbf{\Sigma}_{\hat{\mathbf{p}}_k} = \mathbf{C}_{\mathbf{py}}\mathbf{C}_{\mathbf{yy}}^{-1}\mathbf{C}_{\mathbf{py}}^H. \tag{29b}$$

Note that

$$\lim_{P_p\to\infty}\frac{1}{P_p}\mathbf{C}_{\mathbf{yy}} = \mathbf{B}_k\mathbf{D}_{\tilde{\mathbf{h}}_k}\mathbf{\Sigma}_{\mathbf{g}_k}\mathbf{D}_{\tilde{\mathbf{h}}_k}^H\mathbf{B}_k^H + \mathbf{B}_j\mathbf{D}_{\tilde{\mathbf{q}}_k}\mathbf{\Sigma}_{\mathbf{p}_k}\mathbf{D}_{\tilde{\mathbf{q}}_k}^H\mathbf{B}_j^H, \tag{30}$$

which then translates to

$$\lim_{P_p\to\infty}\mathbf{\Sigma}_{\hat{\mathbf{g}}_k} = \mathbf{\Sigma}_{\mathbf{g}_k}\mathbf{D}_{\tilde{\mathbf{h}}_k}^H\mathbf{B}_k^H\Big(\mathbf{B}_k\mathbf{D}_{\tilde{\mathbf{h}}_k}\mathbf{\Sigma}_{\mathbf{g}_k}\mathbf{D}_{\tilde{\mathbf{h}}_k}^H\mathbf{B}_k^H + \mathbf{B}_j\mathbf{D}_{\tilde{\mathbf{q}}_k}\mathbf{\Sigma}_{\mathbf{p}_k}\mathbf{D}_{\tilde{\mathbf{q}}_k}^H\mathbf{B}_j\Big)^{-1}\mathbf{B}_k\mathbf{D}_{\tilde{\mathbf{h}}_k}\mathbf{\Sigma}_{\mathbf{g}_k}, \tag{31a}$$

$$\lim_{P_p\to\infty}\mathbf{\Sigma}_{\hat{\mathbf{p}}_k} = \mathbf{\Sigma}_{\mathbf{p}_k}\mathbf{D}_{\tilde{\mathbf{q}}_k}^H\mathbf{B}_j^H\Big(\mathbf{B}_k\mathbf{D}_{\tilde{\mathbf{h}}_k}\mathbf{\Sigma}_{\mathbf{g}_k}\mathbf{D}_{\tilde{\mathbf{h}}_k}^H\mathbf{B}_k^H + \mathbf{B}_j\mathbf{D}_{\tilde{\mathbf{q}}_k}\mathbf{\Sigma}_{\mathbf{p}_k}\mathbf{D}_{\tilde{\mathbf{q}}_k}^H\mathbf{B}_j\Big)^{-1}\mathbf{B}_j\mathbf{D}_{\tilde{\mathbf{q}}_k}\mathbf{\Sigma}_{\mathbf{p}_k}. \tag{31b}$$

For Scheme 1, if we insert $\mathbf{B}_k$ and $\mathbf{B}_k^H$ inside the matrix inversion using their pseudoinverses, we get

$$\lim_{P_p\to\infty}(\mathbf{B}_k^H\mathbf{B}_k)^{-1}\mathbf{B}_k^H\mathbf{C}_{\mathbf{yy}}\mathbf{B}_k(\mathbf{B}_k^H\mathbf{B}_k)^{-1} = \mathbf{D}_{\tilde{\mathbf{h}}_k}\mathbf{\Sigma}_{\mathbf{g}_k}\mathbf{D}_{\tilde{\mathbf{h}}_k}^H, \tag{32a}$$

$$\lim_{P_p\to\infty}(\mathbf{B}_j^H\mathbf{B}_j)^{-1}\mathbf{B}_j^H\mathbf{C}_{\mathbf{yy}}\mathbf{B}_k(\mathbf{B}_j^H\mathbf{B}_j)^{-1} = \mathbf{D}_{\tilde{\mathbf{q}}_k}\mathbf{\Sigma}_{\mathbf{p}_k}\mathbf{D}_{\tilde{\mathbf{q}}_k}^H, \tag{32b}$$

since $\mathbf{B}_1^H\mathbf{B}_2 = \mathbf{0}$. Observe that this yields

$$\lim_{P_p\to\infty}\mathbf{\Sigma}_{\hat{\mathbf{g}}_k} = \mathbf{\Sigma}_{\mathbf{g}_k}\mathbf{D}_{\tilde{\mathbf{h}}_k}^H(\mathbf{D}_{\tilde{\mathbf{h}}_k}\mathbf{\Sigma}_{\mathbf{g}_k}\mathbf{D}_{\tilde{\mathbf{h}}_k}^H)^{-1}\mathbf{D}_{\tilde{\mathbf{h}}_k}\mathbf{\Sigma}_{\mathbf{g}_k} = \mathbf{\Sigma}_{\mathbf{g}_k}, \tag{33a}$$

$$\lim_{P_p\to\infty}\mathbf{\Sigma}_{\hat{\mathbf{p}}_k} = \mathbf{\Sigma}_{\mathbf{p}_k}\mathbf{D}_{\tilde{\mathbf{q}}_k}^H(\mathbf{D}_{\tilde{\mathbf{q}}_k}\mathbf{\Sigma}_{\mathbf{p}_k}\mathbf{D}_{\tilde{\mathbf{q}}_k}^H)^{-1}\mathbf{D}_{\tilde{\mathbf{q}}_k}\mathbf{\Sigma}_{\mathbf{p}_k} = \mathbf{\Sigma}_{\mathbf{p}_k}. \tag{33b}$$

In contrast, since $\mathbf{B}_1 = \mathbf{B}_2$ for the baseline scheme, we obtain the results shown in in Section III. The resulting asymptotic covariances of the estimators are summarized in (34). In Section VII, the statistics of the effective channel conditioned on the channel estimates will be important for determining the lower bound for channel capacity.

VII. CAPACITY LOWER BOUND FOR RELIABLE COMMUNICATION UNDER IMPERFECT CSI

While the previous section demonstrates the impact of removing pilot contamination on the channel estimation performance, examining the benefits of this for data transmission performance is also important. To this end, we compute a lower bound on the ergodic capacity based on the imperfect CSI obtained in the previous section via uplink pilot transmission in this section. In particular, we consider the channel capacity for the two schemes we have specified in Section VI. We first recall important results on the relation between channel capacity and CSI for single input single output (SISO) channels, which will be useful in the sequel.

A. CAPACITY LOWER BOUND OF A SISO CHANNEL WITH CHANNEL SIDE INFORMATION

Consider a generic SISO system with the following received signal model:

$$y = hx + w. \tag{35}$$

$$\lim_{P_p\to\infty}\boldsymbol{\Sigma}_{\hat{\mathbf{g}}_k}=\begin{cases}\boldsymbol{\Sigma}_{\mathbf{g}_k} & \text{for Scheme 1,}\\ \boldsymbol{\Sigma}_{\mathbf{g}_k}\mathbf{D}_{\tilde{\mathbf{h}}_k}^H(\mathbf{D}_{\tilde{\mathbf{h}}_k}\boldsymbol{\Sigma}_{\mathbf{g}_k}\mathbf{D}_{\tilde{\mathbf{h}}_k}^H+\underbrace{\mathbf{D}_{\tilde{\mathbf{q}}_k}\boldsymbol{\Sigma}_{\mathbf{p}_k}\mathbf{D}_{\tilde{\mathbf{q}}_k}^H}_{\text{pilot contamination term}})^{-1}\mathbf{D}_{\tilde{\mathbf{h}}_k}\boldsymbol{\Sigma}_{\mathbf{g}_k} & \text{for the baseline scheme,}\end{cases}\tag{34a}$$

$$\lim_{P_p\to\infty}\boldsymbol{\Sigma}_{\hat{\mathbf{p}}_k}=\begin{cases}\boldsymbol{\Sigma}_{\mathbf{p}_k} & \text{for Scheme 1,}\\ \boldsymbol{\Sigma}_{\mathbf{p}_k}\mathbf{D}_{\tilde{\mathbf{q}}_k}^H(\underbrace{\mathbf{D}_{\tilde{\mathbf{h}}_k}\boldsymbol{\Sigma}_{\mathbf{g}_k}\mathbf{D}_{\tilde{\mathbf{h}}_k}^H}_{\text{pilot contamination term}}+\mathbf{D}_{\tilde{\mathbf{q}}_k}\boldsymbol{\Sigma}_{\mathbf{p}_k}\mathbf{D}_{\tilde{\mathbf{q}}_k}^H)^{-1}\mathbf{D}_{\tilde{\mathbf{q}}_k}\boldsymbol{\Sigma}_{\mathbf{p}_k} & \text{for the baseline scheme.}\end{cases}\tag{34b}$$

Suppose that the receiver has partial information on h, denoted by Ω. Then the capacity lower bound is [37, Eq. 2.46]

$$C\geq\mathbb{E}_\Omega\left[\log_2\left(1+\frac{|\mathbb{E}[h|\Omega]|^2}{\mathrm{Var}(h|\Omega)+\mathrm{Var}(w|\Omega)}\right)\right].\tag{36}$$

This bound is valid under three conditions: $\mathbb{E}[w|\Omega]=0$, $\mathbb{E}[xw^*|\Omega]=\mathbb{E}[x|\Omega]\mathbb{E}[w^*|\Omega]$, and $\mathbb{E}[hxw^*|\Omega]=\mathbb{E}[hx|\Omega]\mathbb{E}[w^*|\Omega]$ [37, Section 2.3.5].

B. CAPACITY LOWER BOUND

To maximize gain over the intended channels, the operators configure the RISs based on their channel estimates. That is,

$$\begin{aligned}\hat{\phi}_{kn}&=\arg(h_{kn})+\arg(\hat{g}_{kn}),\\ \hat{\boldsymbol{\Phi}}_k&=\mathrm{diag}\left(e^{-j\hat{\phi}_{k1}},\ldots,e^{-j\hat{\phi}_{kN}}\right),\end{aligned}\tag{37}$$

where $\arg(\cdot)$ denotes the angle (or argument) of the complex number.

1) SCHEME 1

When the scheme described in Section A is used during channel estimation and the beamforming vector is left unchanged throughout data transmission, the following received data signal model arises:

$$y_1=\sqrt{P_d}(\tilde{\mathbf{h}}_1^T\boldsymbol{\Phi}_1\mathbf{g}_1+\tilde{\mathbf{q}}_1^T\boldsymbol{\Phi}_2\mathbf{p}_1)x_1+w_1,\tag{38a}$$

$$y_2=\sqrt{P_d}(\tilde{\mathbf{h}}_2^T\boldsymbol{\Phi}_2\mathbf{g}_2+\tilde{\mathbf{q}}_2^T\boldsymbol{\Phi}_1\mathbf{p}_2)x_2+w_2.\tag{38b}$$

For this scheme, we have to consider both paths and the estimates of both $\mathbf{g}_k$ and $\mathbf{p}_k$. Therefore, we should define the overall SISO channel as

$$v_k\triangleq\sqrt{P_d}(\tilde{\mathbf{h}}_k^T\hat{\boldsymbol{\Phi}}_k\mathbf{g}_k+\tilde{\mathbf{q}}_k^T\hat{\boldsymbol{\Phi}}_j\mathbf{p}_k).\tag{39}$$

To derive the capacity bound, we need to identify the available channel side information Ω. For this scheme, we estimate both $\mathbf{g}_k$ and $\mathbf{p}_k$, therefore, we can deduce that Ω is $\hat{\mathbf{g}}_k$ and $\hat{\mathbf{p}}_k$. Consequently, the expressions we have to evaluate to obtain the capacity lower bound are $\mathbb{E}[v_k|\hat{\mathbf{g}}_k,\hat{\mathbf{p}}_k]$ and $\mathrm{Var}(v_k|\hat{\mathbf{g}}_k,\hat{\mathbf{p}}_k)$. First, consider the conditional mean of the overall SISO channel:

$$\begin{aligned}&\mathbb{E}[v_k|\hat{\mathbf{g}}_k,\hat{\mathbf{p}}_k]=\\ &\quad\sqrt{P_d}(\tilde{\mathbf{h}}_k^T\hat{\boldsymbol{\Phi}}_k\mathbb{E}[\mathbf{g}_k|\hat{\mathbf{g}}_k,\hat{\mathbf{p}}_k]+\tilde{\mathbf{q}}_k^T\hat{\boldsymbol{\Phi}}_j\mathbb{E}[\mathbf{p}_k|\hat{\mathbf{g}}_k,\hat{\mathbf{p}}_k]).\end{aligned}\tag{40}$$

Note that since $\mathbf{B}_1^H\mathbf{B}_2=\mathbf{0}$, the estimation of $\mathbf{g}_k$ and $\mathbf{p}_k$ were separated in the channel estimation step. Therefore, $\mathbf{g}_k$ and $\hat{\mathbf{p}}_k$ are independent. As a result, we can simplify (40) as

$$\mathbb{E}[v_k|\hat{\mathbf{g}}_k,\hat{\mathbf{p}}_k]=\sqrt{P_d}(\tilde{\mathbf{h}}_k^T\hat{\boldsymbol{\Phi}}_k\mathbb{E}[\mathbf{g}_k|\hat{\mathbf{g}}_k]+\tilde{\mathbf{q}}_k^T\hat{\boldsymbol{\Phi}}_j\mathbb{E}[\mathbf{p}_k|\hat{\mathbf{p}}_k]).\tag{41}$$

What remains is to evaluate $\mathbb{E}[\mathbf{g}_k|\hat{\mathbf{g}}_k]$ and $\mathbb{E}[\mathbf{p}_k|\hat{\mathbf{p}}_k]$. To this end, we recall that the MMSE estimator is the conditional mean estimator, that is, the expectations of interest are the MMSE estimates of $\mathbf{g}_k$ based on $\hat{\mathbf{g}}_k$ and $\mathbf{p}_k$ based on $\hat{\mathbf{p}}_k$, respectively. Since the $\mathbf{g}_k$–$\hat{\mathbf{g}}_k$ and $\mathbf{p}_k$–$\hat{\mathbf{p}}_k$ pairs are jointly Gaussian, the MMSE estimates are equivalent to the linear minimum mean squared error (LMMSE) estimates in both cases. As a result, we can evaluate these expectations as follows:

$$\begin{aligned}\mathbb{E}[\mathbf{g}_k|\hat{\mathbf{g}}_k]&=\hat{\mathbf{g}}_k,\\ \mathbb{E}[\mathbf{p}_k|\hat{\mathbf{p}}_k]&=\hat{\mathbf{p}}_k,\end{aligned}\tag{42}$$

since the channel estimation error is independent of the channel itself and is complex Gaussian. Next, we shall consider $\mathrm{Var}(v_k|\hat{\mathbf{g}}_k,\hat{\mathbf{p}}_k)$. We can express this as

$$\begin{aligned}\mathrm{Var}(v_k|\hat{\mathbf{g}}_k,\hat{\mathbf{p}}_k)&=\mathrm{Var}\left(\sqrt{P_d}(\tilde{\mathbf{h}}_k^T\hat{\boldsymbol{\Phi}}_k\mathbf{g}_k+\tilde{\mathbf{q}}_k^T\hat{\boldsymbol{\Phi}}_j\mathbf{p}_k)|\hat{\mathbf{g}}_k,\hat{\mathbf{p}}_k\right),\\ &=P_d\tilde{\mathbf{h}}_k^T\hat{\boldsymbol{\Phi}}_k\,\mathrm{Var}(\mathbf{g}_k|\hat{\mathbf{g}}_k,\hat{\mathbf{p}}_k)\hat{\boldsymbol{\Phi}}_k^H\tilde{\mathbf{h}}_k^*\\ &\quad+P_d\tilde{\mathbf{q}}_k^T\hat{\boldsymbol{\Phi}}_j\,\mathrm{Var}(\mathbf{p}_k|\hat{\mathbf{g}}_k,\hat{\mathbf{p}}_k)\hat{\boldsymbol{\Phi}}_j^H\tilde{\mathbf{q}}_k^*\\ &\quad+2P_d\,\mathrm{Re}\left\{\tilde{\mathbf{h}}_k\hat{\boldsymbol{\Phi}}_k\underbrace{\mathrm{Cov}(\mathbf{g}_k,\mathbf{p}_k|\hat{\mathbf{g}}_k,\hat{\mathbf{p}}_k)}_{=0}\hat{\boldsymbol{\Phi}}_j^H\tilde{\mathbf{q}}_k^*\right\}.\end{aligned}\tag{43}$$

Note that $\mathbf{g}_k$ is independent from $\hat{\mathbf{p}}_k$, hence we can simplify (43) as

$$\begin{aligned}\mathrm{Var}(v_k|\hat{\mathbf{g}}_k,\hat{\mathbf{p}}_k)&=P_d\tilde{\mathbf{h}}_k^T\hat{\boldsymbol{\Phi}}_k\,\mathrm{Var}(\mathbf{g}_k|\hat{\mathbf{g}}_k)\hat{\boldsymbol{\Phi}}_k^H\tilde{\mathbf{h}}_k^*\\ &\quad+P_d\tilde{\mathbf{q}}_k^T\hat{\boldsymbol{\Phi}}_j\,\mathrm{Var}(\mathbf{p}_k|\hat{\mathbf{p}}_k)\hat{\boldsymbol{\Phi}}_j^H\tilde{\mathbf{q}}_k^*.\end{aligned}\tag{44}$$

Then, we can use the same MMSE estimation properties to evaluate $\mathrm{Var}(\mathbf{g}_k|\hat{\mathbf{g}}_k)$ and $\mathrm{Var}(\mathbf{p}_k|\hat{\mathbf{p}}_k)$, which results in

$$\begin{aligned}\mathrm{Var}(\mathbf{g}_k|\hat{\mathbf{g}}_k)&=\mathbb{E}[\mathbf{g}_k\mathbf{g}_k^H]-\mathbb{E}[\mathbf{g}_k\hat{\mathbf{g}}_k^H](\mathbb{E}[\hat{\mathbf{g}}_k\hat{\mathbf{g}}_k^H])^{-1}\mathbb{E}[\hat{\mathbf{g}}_k\mathbf{g}_k^H],\\ &=\boldsymbol{\Sigma}_{\mathbf{g}_k}-\mathbf{C}_{\mathbf{gy}}\mathbf{C}_{\mathbf{yy}}^{-1}\mathbf{C}_{\mathbf{gy}}^H,\end{aligned}\tag{45a}$$

$$\begin{aligned}\mathrm{Var}(\mathbf{p}_k|\hat{\mathbf{p}}_k)&=\mathbb{E}[\mathbf{p}_k\mathbf{p}_k^H]-\mathbb{E}[\mathbf{p}_k\hat{\mathbf{p}}_k^H](\mathbb{E}[\hat{\mathbf{p}}_k\hat{\mathbf{p}}_k^H])^{-1}\mathbb{E}[\hat{\mathbf{p}}_k\mathbf{p}_k^H],\\ &=\boldsymbol{\Sigma}_{\mathbf{p}_k}-\mathbf{C}_{\mathbf{py}}\mathbf{C}_{\mathbf{yy}}^{-1}\mathbf{C}_{\mathbf{py}}^H.\end{aligned}\tag{45b}$$

Note that the analysis for Scheme 1 can be applied to the baseline scheme by adjusting the RIS configurations.

2) SCHEME 2

When the scheme described in Section B is used during channel estimation and the beamforming vector is left unchanged throughout data transmission, the following received data signal model arises:

$$y_1 = \sqrt{P_d}\tilde{\mathbf{h}}_1^T \mathbf{\Phi}_1 \mathbf{g}_1 x_1 + w_1, \tag{46a}$$

$$y_2 = \sqrt{P_d}\tilde{\mathbf{h}}_2^T \mathbf{\Phi}_2 \mathbf{g}_2 x_2 + w_2. \tag{46b}$$

For the signal model in (38), it is shown in [33, Lemma 1] that the conditions for the bound in (36) to hold are satisfied. The same can be shown for (46) following the same steps.

In this scheme, we only estimate $\mathbf{g}_k$, therefore, the channel side information Ω corresponds to $\hat{\mathbf{g}}_k$. We can express this channel estimate as

$$\hat{\mathbf{g}}_k = \mathbf{g}_k + \mathbf{e}_k, \tag{47}$$

where $\mathbf{e}_k \sim \mathcal{CN}(\mathbf{0}, \mathbf{\Sigma}_{\mathbf{e}_k})$ with $\mathbf{\Sigma}_{\mathbf{e}_k}$ computed according to (7). To compute the capacity bound, we first have to define the overall SISO channel, that is,

$$v_k \triangleq \sqrt{P_d}\tilde{\mathbf{h}}_k^T \hat{\mathbf{\Phi}}_k \mathbf{g}_k. \tag{48}$$

Then, we should formulate its mean conditioned on $\mathbf{g}_k$, corresponding to the channel side information Ω in (36):

$$\mathbb{E}[v_k|\hat{\mathbf{g}}_k] = \sqrt{P_d}\tilde{\mathbf{h}}_k^T \hat{\mathbf{\Phi}}_k \mathbb{E}[\mathbf{g}_k|\hat{\mathbf{g}}_k] = \sqrt{P_d}\tilde{\mathbf{h}}_k^T \hat{\mathbf{\Phi}}_k \hat{\mathbf{g}}_k, \tag{49}$$

using the same LMMSE idea as before. Next, we have to evaluate $\mathrm{Var}(v_k|\hat{\mathbf{g}}_k)$, which can be expressed as

$$\begin{aligned}\mathrm{Var}(v_k|\hat{\mathbf{g}}_k) &= \mathrm{Var}\left(\sqrt{P_d}\tilde{\mathbf{h}}_k^T \hat{\mathbf{\Phi}}_k \mathbf{g}_k|\hat{\mathbf{g}}_k\right) \\ &= P_d \tilde{\mathbf{h}}_k^T \hat{\mathbf{\Phi}}_k \,\mathrm{Var}(\mathbf{g}_k|\hat{\mathbf{g}}_k) \hat{\mathbf{\Phi}}_k^H \tilde{\mathbf{h}}_k^*. \end{aligned} \tag{50}$$

What remains is to evaluate $\mathrm{Var}(\mathbf{g}_k|\hat{\mathbf{g}}_k)$, which can be done by using the same LMMSE idea as before:

$$\begin{aligned}\mathrm{Var}(\mathbf{g}_k|\hat{\mathbf{g}}_k) &= \mathbb{E}[\mathbf{g}_k\mathbf{g}_k^H] - \mathbb{E}[\mathbf{g}_k\hat{\mathbf{g}}_k^H](\mathbb{E}[\hat{\mathbf{g}}_k\hat{\mathbf{g}}_k^H])^{-1}\mathbb{E}[\hat{\mathbf{g}}_k\mathbf{g}_k^H], \\ &= \mathbf{\Sigma}_{\mathbf{g}_k} - \mathbf{C}_{\mathbf{gy}}\mathbf{C}_{\mathbf{yy}}^{-1}\mathbf{C}_{\mathbf{gy}}^H, \end{aligned} \tag{51}$$

which provides $\mathrm{Var}(v_k|\hat{\mathbf{g}}_k)$ in closed form. Note that w_k is independent of the channels and their estimates; therefore, it is obvious that $\mathrm{Var}(w_k|\Omega) = \sigma_w^2$. Since we also provided the closed-form expressions for $\mathbb{E}[v_k|\Omega]$ and $\mathrm{Var}(v_k|\Omega)$, we have the argument of the expectation in (36) in closed form. The final expressions for the capacity lower bound are shown in (52).

C. ERGODIC CAPACITY

For both schemes, achieving perfect CSI is possible when the channel estimation SNR is sufficiently large since the pilot contamination is removed. Therefore, it is meaningful to consider the channel capacity itself under perfect CSI as a benchmark. Note that we consider the ergodic capacity since there are fading channel components. In addition, we assume that both operators configure their RISs so that

$$\boldsymbol{\phi}_1 = \exp\Big(-j(\arg(\tilde{\mathbf{h}}_1) + \arg(\mathbf{g}_1))\Big), \tag{53a}$$

$$\boldsymbol{\phi}_2 = \exp\Big(-j(\arg(\tilde{\mathbf{h}}_2) + \arg(\mathbf{g}_2))\Big). \tag{53b}$$

Recall that we had defined the effective SISO channel for the two schemes as v_k. By plugging in the definitions of v_k into

$$C_k = \mathbb{E}\left[\log_2\left(1 + \frac{|v_k|^2}{\sigma_w^2}\right)\right], \tag{54}$$

the ergodic capacity for the scheme of interest can be obtained.

D. Summary of analytical results

The closed-form analytical results in this article are obtained by using several equations from the previous discussion. In this subsection, we provide two tables that summarize how to use these equations to obtain the channel estimation error covariance matrix and the capacity lower bound for each scheme with pure-LOS and unstructured RIS-BS channels. In Table 3, we provide the summary for the channel estimation error covariance matrix. In Table 4, we provide the results for the capacity lower bound and the ergodic capacity.

VIII. EXTENSION TO MULTIPLE USERS

The focus of this paper is on the idea of null forming towards the interfering channel to mitigate inter-operator pilot contamination. Therefore, we considered a single user per operator case to improve the readability of this manuscript. In this section, however, we briefly describe how to generalize the system model in Section II for multiple users.

Suppose that each operator serves R_k users. Note that we need to have $R_1, R_2 \leq \min(M, N)$ since the overall MIMO channel's rank is limited by N. In addition, we can no longer consider the pure-LOS case since the RIS-BS links would be rank-1 and hence would be unable to support $R_k > 1$ users. Therefore, we make the assumption that $R_1, R_2 \leq \min(M, N)$ and $\mathrm{rank}(\mathbf{H}_k) \geq R, \mathrm{rank}(\mathbf{Q}_k) \geq R$ for $k = 1, 2$, that is, all RIS-BS channels have at least R non-zero singular values. With this in mind, we can express the multi-user version of (1), the R_k-dimensional received pilot signal, as

$$\mathbf{y}_{pk}[l] = \sqrt{P_p}\mathbf{V}_k(\mathbf{H}_k\mathbf{\Phi}_k[l]\mathbf{G}_k + \mathbf{Q}_k\mathbf{\Phi}_j[l]\mathbf{P}_k)\mathbf{s}_k[l] + \underbrace{\mathbf{V}_k\mathbf{n}_k[l]}_{\triangleq \mathbf{w}_k[l]}, \tag{55}$$

where the r-th row of $\mathbf{V}_k \in \mathbb{C}^{R_k \times M}$ contains the receive beamforming vector that outputs the r-th user's received signal. $\mathbf{G}_k, \mathbf{P}_k \in \mathbb{C}^{N \times R_k}$ denote the UEs-RIS channels whose columns contain the individual users' channels to the RIS. $\mathbf{s}_k[l] \in \mathbb{C}^{R_k}$ is the vector of pilots transmitted by the UEs at the l-th time instant. By defining the effective RIS-BS channels $\tilde{\mathbf{H}}_k \triangleq \mathbf{V}_k\mathbf{H}_k \in \mathbb{C}^{R_k \times N}$ and $\tilde{\mathbf{Q}}_k \triangleq \mathbf{V}_k\mathbf{Q}_k \in \mathbb{C}^{R_k \times N}$, we can rewrite (55) as

$$\mathbf{y}_{pk}[l] = \sqrt{P_p}(\tilde{\mathbf{H}}_k\mathbf{\Phi}_k[l]\mathbf{G}_k + \tilde{\mathbf{Q}}_k\mathbf{\Phi}_j[l]\mathbf{P}_k)\mathbf{s}_k[l] + \mathbf{w}_k[l]. \tag{56}$$

To represent the ensemble of transmitted pilots more clearly, we first define $\mathbf{S}_{\mathbf{\Phi}_k}[l] \triangleq \begin{bmatrix} s_1[l]\boldsymbol{\phi}_k[l] & \dots & s_{R_k}[l]\boldsymbol{\phi}_k[l] \end{bmatrix} \in \mathbb{C}^{1 \times R_k N}$. This term represents the combined time-dependent effect of the transmitted pilot signals and the utilized RIS

$$C_k \geq \begin{cases} \mathbb{E}\left[\log_2\left(1+\frac{\left|\tilde{\mathbf{h}}_k\hat{\mathbf{\Phi}}_k\hat{\mathbf{g}}_k+\tilde{\mathbf{q}}_k\hat{\mathbf{\Phi}}_j\hat{\mathbf{p}}_k\right|^2}{\tilde{\mathbf{h}}_k^T\hat{\mathbf{\Phi}}_k(\mathbf{\Sigma}_{\mathbf{g}_k}-\mathbf{C}_{\mathbf{gy}}\mathbf{C}_{\mathbf{yy}}^{-1}\mathbf{C}_{\mathbf{gy}}^H)\hat{\mathbf{\Phi}}_k^H\tilde{\mathbf{h}}_k^*+\tilde{\mathbf{q}}_k^T\hat{\mathbf{\Phi}}_j(\mathbf{\Sigma}_{\mathbf{p}_k}-\mathbf{C}_{\mathbf{py}}\mathbf{C}_{\mathbf{yy}}^{-1}\mathbf{C}_{\mathbf{py}}^H)\hat{\mathbf{\Phi}}_j^H\tilde{\mathbf{q}}_k^*+\frac{\sigma_w^2}{P_d}}\right)\right], & \text{for Scheme 1,} \\ \mathbb{E}\left[\log_2\left(1+\frac{\tilde{\mathbf{h}}_k\hat{\mathbf{\Phi}}_k\hat{\mathbf{g}}_k\hat{\mathbf{g}}_k^H\hat{\mathbf{\Phi}}_k^H\tilde{\mathbf{h}}_k^*}{\tilde{\mathbf{h}}_k^T\hat{\mathbf{\Phi}}_k(\mathbf{\Sigma}_{\mathbf{g}_k}-\mathbf{C}_{\mathbf{gy}}\mathbf{C}_{\mathbf{yy}}^{-1}\mathbf{C}_{\mathbf{gy}}^H)\hat{\mathbf{\Phi}}_k^H\tilde{\mathbf{h}}_k^*+\frac{\sigma_w^2}{P_d}}\right)\right], & \text{for Scheme 2.} \end{cases} \tag{52}$$

TABLE 3: Summary of channel estimation error covariance matrices for each scheme with pure-LOS and unstructured RIS-BS channels.

Scheme	Error Covariance Matrix (Pure-LOS)	Error Covariance Matrix (Unstructured)
Baseline	(9), and (10) for high SNR; $\mathbf{v}_k$ as in (13)	(9), and (10) for high SNR; $\mathbf{v}_k$ as in (21)
Scheme 1	(28), and (33) for high SNR; $\mathbf{v}_k$ as in (13)	(28), and (33) for high SNR; $\mathbf{v}_k$ as in (21)
Scheme 2	(28), and (33) for high SNR; $\mathbf{v}_k$ as in (16)	(28), and (33) for high SNR; $\mathbf{v}_k$ as in (24)

TABLE 4: Summary of capacity bound expressions for each scheme with pure-LOS and unstructured RIS-BS channels. Note that Schemes 1 and 2 have different error covariance matrices since different $\mathbf{v}_k$ results in different $\tilde{\mathbf{h}}_k$ and $\tilde{\mathbf{q}}_k$.

Scheme	Capacity Bound (Pure-LOS)	Capacity Bound (Unstructured)
Baseline	[33, Eq. 55]; $\mathbf{v}_k$ as in (13), use $\tilde{\mathbf{h}}_k$ and $\tilde{\mathbf{q}}_k$ instead of $\mathbf{h}_k$ and $\mathbf{q}_k$	[33, Eq. 55]; $\mathbf{v}_k$ as in (21), use $\tilde{\mathbf{h}}_k$ and $\tilde{\mathbf{q}}_k$ instead of $\mathbf{h}_k$ and $\mathbf{q}_k$
Scheme 1	(52); $\mathbf{v}_k$ as in (13)	(52), $\mathbf{v}_k$ as in (21)
Scheme 2	(52), $\mathbf{v}_k$ as in (16)	(52); $\mathbf{v}_k$ as in (24)

configurations. Then by defining $\tilde{\mathbf{S}}_{\mathbf{\Phi}_k}[l] \triangleq \mathbf{I}_{R_k} \otimes \mathbf{S}_{\mathbf{\Phi}_k}[l] \in \mathbb{C}^{R_k \times R_k^2 N}$, $\tilde{\mathbf{g}}_k \triangleq \text{vec}(\mathbf{G}_\text{k}) \in \mathbb{C}^{\text{R}_\text{k}\text{N}}$ and $\tilde{\mathbf{p}}_k \triangleq \text{vec}(\mathbf{P}_\text{k}) \in \mathbb{C}^{\text{R}_\text{k}\text{N}}$, we can rewrite (56) as

$$\mathbf{y}_{pk}[l] = \sqrt{P_p}(\tilde{\mathbf{S}}_{\mathbf{\Phi}_k}[l]\mathbf{D}_{\tilde{\mathbf{H}}_k}\tilde{\mathbf{g}}_k + \tilde{\mathbf{S}}_{\mathbf{\Phi}_j}[l]\mathbf{D}_{\tilde{\mathbf{Q}}_k}\tilde{\mathbf{p}}_k + \mathbf{w}_k[l] \in \mathbb{C}^{R_k}. \tag{57}$$

Note that (57) has a similar structure with (3) since l-dependent terms are on the left-most part of matrix multiplications. Hence, we can stack the observations over $l = 1, \ldots, L$ vertically to obtain

$$\mathbf{Y}_{pk} = \sqrt{P_p}(\mathbf{B}_k\mathbf{D}_{\tilde{\mathbf{H}}_k}\tilde{\mathbf{g}}_k + \mathbf{B}_j\mathbf{D}_{\tilde{\mathbf{Q}}_k}\tilde{\mathbf{p}}_k) + \mathbf{W}_k[l] \in \mathbb{C}^{R_k}, \tag{58}$$

where $\mathbf{B}_k \triangleq \begin{bmatrix}\tilde{\mathbf{S}}_{\mathbf{\Phi}_k}^T[1] & \tilde{\mathbf{S}}_{\mathbf{\Phi}_k}^T[2] & \ldots & \tilde{\mathbf{S}}_{\mathbf{\Phi}_k}^T[L]\end{bmatrix}^T \in \mathbb{C}^{R_k L \times R_k^2 N}$.

This time, the individual rows of $\mathbf{V}_k$ will undergo the beamforming design processes described in Section V. To separate the main lobes of the beams, each row will have to be assigned one of the right singular vectors of $\mathbf{H}_k$, and each row will undergo the null forming process in case Scheme 2 is used. If $\mathbf{V}_k = \begin{bmatrix}\mathbf{v}_{k,1}^T & \ldots & \mathbf{v}_{k,R_k}^T\end{bmatrix}^T$, then the beamforming process in Section A becomes:

$$\mathbf{v}_{k,1}^T = \boldsymbol{\gamma}_{k,1}^H \tag{59a}$$
$$\mathbf{v}_{k,2}^T = \boldsymbol{\gamma}_{k,2}^H \tag{59b}$$
$$\vdots$$
$$\mathbf{v}_{k,R_k}^T = \boldsymbol{\gamma}_{k,R_k}^H, \tag{59c}$$

where $\boldsymbol{\gamma}_{k,1}, \ldots, \boldsymbol{\gamma}_{k,R_k}$ are the R_k right singular vectors of $\mathbf{H}_k$ corresponding to the R_k largest singular values of $\mathbf{H}_k$. Starting from this point, every vector would undergo the process in Section B if null forming is to be utilized.

IX. NUMERICAL RESULTS

In this section, we discuss numerical examples for the channel estimation and capacity lower bound analysis to demonstrate the benefits of mitigating inter-operator pilot contamination. In Section A, we provide the numerical results for channel estimation for the two schemes for pure-LOS and unstructured RIS-BS channels. In Section B, we simulate the outer expectation over multiple channel realizations and compare the two schemes for pure-LOS and unstructured channels. To show that eliminating inter-operator pilot contamination is necessary, we construct a baseline scheme that transmits $L = N$ pilots and uses the same beamformer as Scheme 1. That is, the baseline scheme does not eliminate inter-operator pilot contamination by receive beamforming or orthogonalizing RIS configurations. It has to be noted that regularized zero forcing (RZF) beamforming, a state-of-the-art method, is not included in the analysis as our numerical results (not shown here) indicate that Scheme 2 provides the same performance as the RZF approach.

A. CHANNEL ESTIMATION BASED ON CORRELATED RAYLEIGH FADING PRIORS

In this section, we provide numerical examples for estimating correlated Rayleigh fading channels. We consider the two schemes described in Sections A and B, along with the baseline scheme described at the beginning of this section. For different P_p, we compute the normalized mean squared error (NMSE) of MMSE channel estimation, which is given

by

$$\text{NMSE}_{\mathbf{g}_k} = \frac{\text{tr}(\mathbf{\Sigma}_{\mathbf{e}_{\mathbf{g}_k}})}{\text{tr}(\mathbf{\Sigma}_{\mathbf{g}_k})}, \tag{60a}$$

$$\text{NMSE}_{\mathbf{p}_k} = \frac{\text{tr}(\mathbf{\Sigma}_{\mathbf{e}_{\mathbf{p}_k}})}{\text{tr}(\mathbf{\Sigma}_{\mathbf{p}_k})}, \tag{60b}$$

where $\mathbf{\Sigma}_{\mathbf{e}_{\mathbf{g}_k}}$ and $\mathbf{\Sigma}_{\mathbf{e}_{\mathbf{p}_k}}$ are as in (7). In Figs. 2 and 3, the channel estimation NMSEs for $\mathbf{g}_1$ and $\mathbf{p}_1$[†] are shown for $N = 64$ and $M = 256$. The list of parameters used for these figures is provided in Table 6. Note that although our analysis is valid for any positive definite covariance matrix of $\mathbf{g}_k$ and $\mathbf{p}_k$, we consider i.i.d. Rayleigh fading in this section. That is, $\mathbf{g}_k, \mathbf{p}_k \sim \mathcal{CN}(\mathbf{0}, \mathbf{I}_N)$.

TABLE 5: Parameters used in Figs. 2 and 3.

Parameter	Value
Transmit pilot power (P_p)	$-30, -25, \ldots, 60$ dBm
Carrier frequency (f_c)	30 GHz, 28 GHz[‡]
UE-RIS path loss	-80 dB
RIS-BS path loss	-60 dB
Noise variance (σ_w^2)	-90 dBm
Number of BS antennas (M)	64
Number of RIS elements (N)	256
Number of pilot transmissions (L)	N, $2N$

The results provided in Figs. 2 and 3 are generated by using the minimum number of pilots required for each scheme. This raises the question of whether these results could be improved or not by simply adding more pilots. To answer this question, we provide the numerical results in Fig. 4. Using the same parameters as in Table 6 and fixing P_p to 0 dBm and 30 dBm, we plot the NMSE for different multiples of L, ranging from $L = N$ to $L = 8N$. Note that we start the plot from $L = 2N$ for Scheme 1 as $L \geq 2N$ is the requirement for this scheme to work.

In Fig. 2, note that $\mathbf{p}_1$ has a much higher NMSE than $\mathbf{g}_1$ for both Scheme 1 and the baseline scheme. This is because the BS beamforms towards $\mathbf{H}_1$ rather than $\mathbf{Q}_1$ in both; therefore, the channel estimation SNR is boosted significantly. Since both $\mathbf{H}_1$ and $\mathbf{Q}_1$ are pure-LOS channels, they are also directive and are highly separated angularly. That is, when $\mathbf{v}_1$ is dedicated to obtain the maximum gain from $\mathbf{H}_1$, i.e., maximizing $\|\tilde{\mathbf{h}}_1\|^2$, $\|\tilde{\mathbf{q}}_1\|^2$ decreases substantially even in the absence of nullforming. This is because the dominant singular vector of $\mathbf{Q}_1$ does not align with that of $\mathbf{H}_1$. Therefore, beamforming towards $\mathbf{H}_1$ decreases the received pilot SNR along the $\mathbf{p}_1$-$\mathbf{Q}_1$ path significantly. In addition, note that $\mathbf{g}_1$ is estimated more accurately under Scheme 1 compared to Scheme 2. This is because null forming towards $\mathbf{Q}_1$ weakens the main lobe of the beam, i.e., $\mathbf{v}_1$ aligns with the dominant singular vector of $\mathbf{H}_1$ suboptimally as opposed to Scheme 1. Also note that the baseline scheme performs similarly with Scheme 2 until $P_p = 40$ dBm and starts to converge to a finite value. It has to be noted that the baseline scheme uses the same beamforming vector as Scheme 1, therefore, the difference between Scheme 1 and the baseline scheme's performance in estimating $\mathbf{g}_1$ comes from the fact that $L = 2N$ pilots are used in Scheme 1 while $L = N$ pilots are used in the baseline scheme. Therefore, the gap between them is around 3 dB.

In Fig. 3, note that Schemes 1 & 2 perform similarly with very minor differences. In contrast, the baseline scheme fails to provide useful channel estimates. Compared to the pure-LOS case, the baseline scheme has much worse performance, starting to show the impact of inter-operator pilot contamination at around 5 dBm. After around 20 dBm, the NMSE of the baseline scheme converges to a constant, which is the pilot contamination term. This is again due to the high angular separation between $\mathbf{Q}_1$ and $\mathbf{H}_1$ in the pure-LOS case. This angular separation was decreasing the gain of the $\mathbf{p}_1$–$\mathbf{Q}_1$ path substantially. However, the arbitrary structure of $\mathbf{H}_1$ and $\mathbf{Q}_1$ prevents this phenomenon in this case. For the very same reason, the NMSE of estimating $\mathbf{p}_1$ and $\mathbf{g}_1$ under Scheme 1 does not differ as much as it did in the pure-LOS case.

Note that when there is pure-LOS between the RISs and the BSs, the baseline scheme performs similarly to Scheme 2 up to a transmit power of $P_p = 40$ dBm as shown in Fig. 2. On the other hand, the baseline scheme has inferior performance when the RIS-BS links do not exhibit any structure, as shown in Fig. 3. This is a consequence of the beam structures for the two cases. For the pure-LOS case, the intended and interfering channels are already well-separated in space, and the absence of nullforming does not degrade the performance much. That is, there is much less inter-operator pilot contamination when there is pure-LOS between the RISs and the BSs when compared to the case where the RIS-BS channels do not exhibit any structure.

The results in Figs. 2 and 3 demonstrate the significance of the non-vanishing pilot contamination terms in (10). That is, at high P_p, the estimator covariances do not converge to the parameter covariances, implying that obtaining perfect estimates is not possible. In contrast, when Schemes 1 and 2 are applied, these covariances converge to the parameter covariances.

In Scheme 1, beamforming is fully focused on collecting energy from the $\mathbf{g}_k$–$\mathbf{H}_k$ path, and this weakens the interfering signal energy coming over the $\mathbf{p}_k$–$\mathbf{Q}_k$ path if $\mathbf{H}_k$ and $\mathbf{Q}_k$ could be separated over space, as in the case of pure-LOS. The results in Fig. 2 show that when the angular separation between $\mathbf{H}_k$ and $\mathbf{Q}_k$ is substantial, the energy sacrificed from the main lobe of the beam for null forming is greater than the gain provided by interference cancellation. In contrast, the results in Fig. 3 follow a different trend. The angular separation is not as large as that in the pure-LOS case, hence the interference nulled by Scheme 2 is substantial.

[†]Note that the same results can also be obtained for $k = 2$; however, we show the results for the first operator to keep the figures readable.

TABLE 6: Parameters used in Figs. 2 and 3.

Parameter	Value
Transmit pilot power (P_p)	$-30, -25, \ldots, 60$ dBm
Carrier frequency (f_c)	30 GHz, 28 GHz[§]
UE-RIS path loss	-80 dB
RIS-BS path loss	-60 dB
Noise variance (σ_w^2)	-90 dBm
Number of BS antennas (M)	64
Number of RIS elements (N)	256
Number of pilot transmissions (L)	N, $2N$

When the transmit power is relatively low, the received signal power is a scarce resource. Scheme 1 optimally captures the received signal as opposed to Scheme 2 and hence performs better when the transmit pilot power is low. Note that around $P_p = 40$ dBm, the two schemes start to perform similarly since the difference between the gains of the main lobes of the two schemes becomes less significant.

In Figs. 4a and 4c, note that as the number of pilots increases, the NMSE decreases for all schemes. This is because the captured pilot power at the BS is the limiting factor for channel estimation when $P_p = 0$ dBm. Increasing the number of pilots increases the captured power at the BS, hence it decreases the NMSE per unknown channel component. In contrast, the performance of the baseline scheme does not improve when the number of pilots increases in Fig. 4d since the captured pilot power is no longer the limiting factor here, but rather the inter-operator pilot contamination. This figure shows that inter-operator pilot contamination cannot be mitigated by transmitting more pilots when the baseline scheme is used. In Fig. 4b, we still see some improvement in the performance of the baseline scheme. However, note that while the three schemes perform the same in Fig. 4a, the baseline scheme starts to be outperformed as the number of pilots increases in Fig. 4b since inter-operator pilot contamination starts to become the limiting factor for this setup. Also note that since the NMSE is inversely proportional to L, increasing L gives diminishing returns for channel estimation.

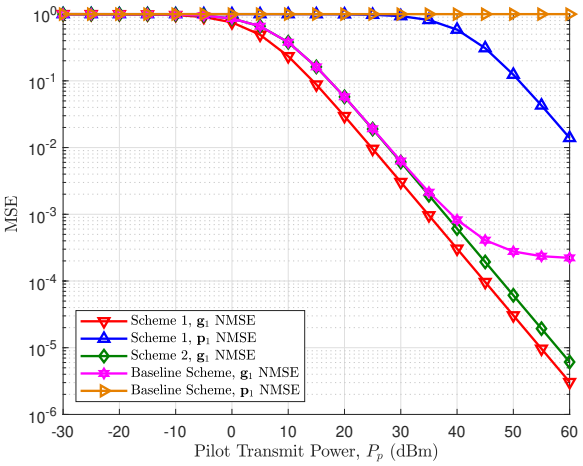

FIGURE 2: Channel estimation NMSE of $\mathbf{g}_1$ and $\mathbf{p}_1$ for the two schemes when $\mathbf{H}_1$ and $\mathbf{Q}_1$ are pure-LOS channels.

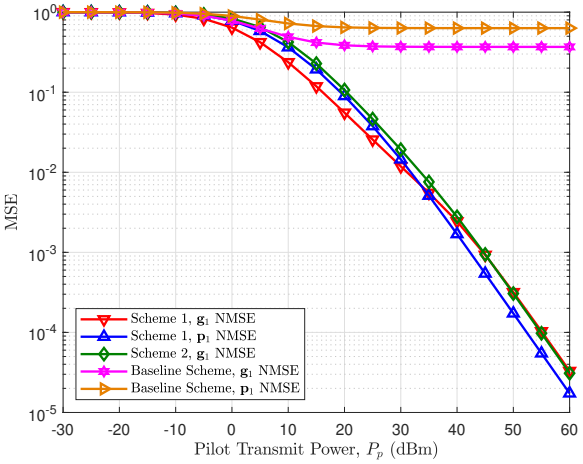

FIGURE 3: Channel estimation NMSE of $\mathbf{g}_1$ and $\mathbf{p}_1$ for the two schemes when $\mathbf{H}_1$ and $\mathbf{Q}_1$ do not exhibit any structure.

B. CAPACITY LOWER BOUND FOR RELIABLE COMMUNICATION UNDER IMPERFECT CSI

In this section, we provide numerical examples for the capacity lower bound expression in Section VII. While the results in Section A demonstrated that Scheme 1 provides higher capacity, one should consider the fact that Scheme 2 and the baseline scheme uses half of the pilots used in Scheme 1, i.e., $L = N$ instead of $L = 2N$. To treat the two schemes fairly, we consider a fictitious slot structure where L pilot transmissions are followed by D data transmissions. During the data transmission phase, we assume that the capacity bounds or the ergodic capacities apply, and hence we compute the throughput over $L + D$ channel uses. We assume that a single coherence block lasts for $3N$ transmissions. For both schemes, we use the minimum number of pilots, i.e., $L = 2N$ for Scheme 1 and $L = N$ for Scheme 2 and the baseline scheme. Then, we consider the spectral efficiency (SE) and its lower bound. Suppose that the channel capacity is C, then the SE is $\frac{D}{D+L}C$ since we use the channel $D + L$ times and we transmit data in D of these instances. Since a single coherence block lasts $3N$ transmissions, we perform $D = N$ data transmissions in Scheme 1 and $D = 2N$ data transmissions in Scheme 2 and the baseline scheme. Consequently, we transmit data $1/3$ of the time in Scheme 1 and $2/3$ of the time in Scheme 2 and the baseline scheme.

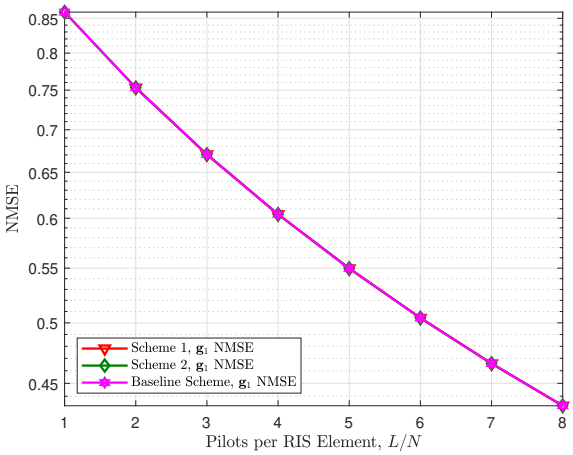

(a) Pure-LOS RIS-BS channels, $P_p = 0$ dBm

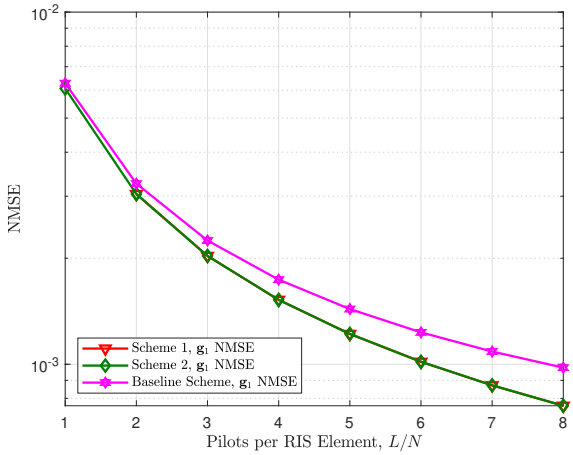

(b) Pure-LOS RIS-BS channels, $P_p = 30$ dBm

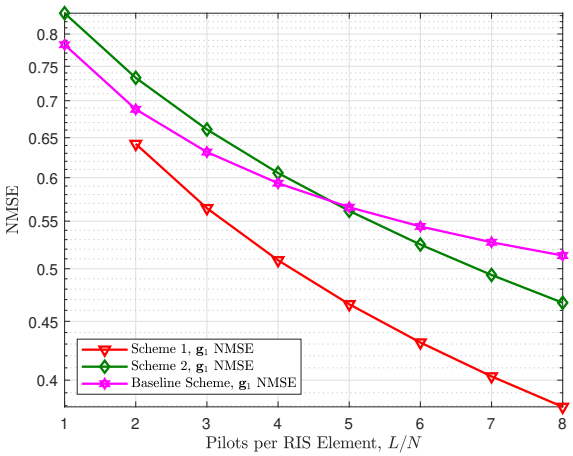

(c) Unstructured RIS-BS channels, $P_p = 0$ dBm

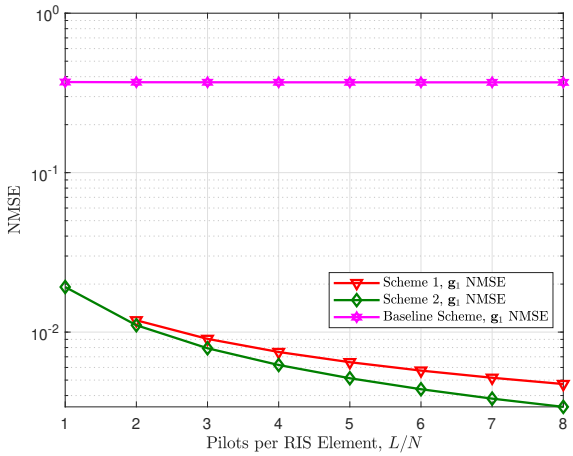

(d) Unstructured RIS-BS channels, $P_p = 30$ dBm

FIGURE 4: Channel estimation NMSE for different number of pilots per RIS element for pure-LOS and unstructured RIS-BS scenarios for two different pilot transmit powers, P_p.

TABLE 7: Parameters used in Figs. 5 and 6.

Parameter	Value
Transmit data power (P_d)	$-30, -10, \ldots, 130$ dBm
Transmit pilot power (P_p)	P_d[†]
UE-RIS path loss	-80 dB
RIS-BS path loss	-60 dB
Noise variance (σ_w^2)	-90 dBm
Number of BS antennas (M)	256
Number of RIS elements (N)	64
Number of pilot transmissions (L)	N, $2N$
Number of data transmissions (D)	$2N$, N

[†]Each point of the capacity bound plot in Fig. 5 and 6 corresponds to the case when the pilot and data transmission powers are equal to each other. On the other hand, the ergodic capacity is based on perfect CSI.

In Figs. 5 and 6, note that the capacity bound curves for Schemes 1 and 2 follow the ergodic capacity curves closely, showing that perfect CSI is indeed achievable at sufficiently high pilot transmission power. In contrast, the capacity lower bound for the baseline scheme diverges from its corresponding ergodic capacity curve after $P_d = 30$ dBm for Fig. 5 and $P_d = -10$ dBm for Fig. 6.

In Fig. 5, the baseline scheme outperforms Schemes 1 and 2 at low transmit powers since the signal power is scarce, and the baseline scheme neither sacrifices its beam's main lobe nor doubles the number of pilots. After $P_d = 30$ dBm, however, the baseline scheme is penalized by the inter-operator pilot contamination despite the strong spatial separation between the intended and the interfering channels. Consequently, Schemes 1 and 2 outperform the baseline scheme starting from $P_d = 45$ dBm and $P_d = 90$ dBm,

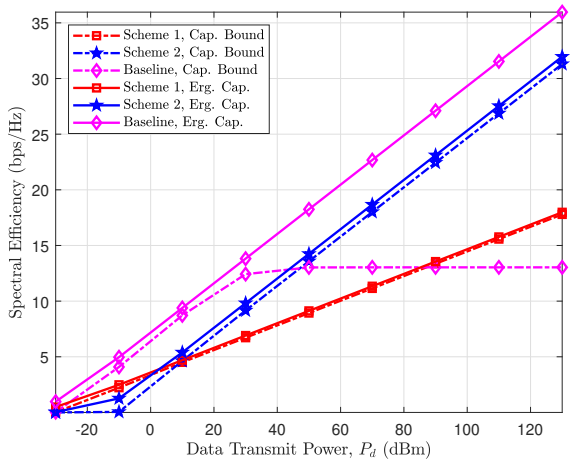

FIGURE 5: Capacity lower bound and the ergodic capacity for the two schemes and the baseline scheme when $\mathbf{H}_1$ and $\mathbf{Q}_1$ are pure-LOS. The dashed lines represent the capacity lower bound in (36) and the solid lines represent the ergodic capacity in (54).

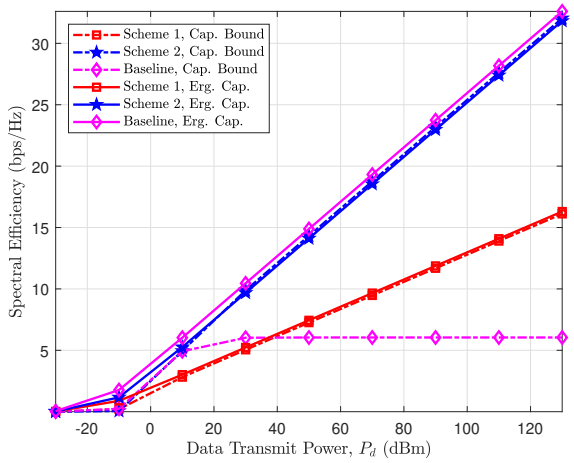

FIGURE 6: Capacity lower bound and the ergodic capacity for the two schemes and the baseline scheme when $\mathbf{H}_1$ and $\mathbf{Q}_1$ do not exhibit any structure. The dashed lines represent the capacity lower bound in (36) and the solid lines represent the ergodic capacity in (54).

respectively. Although Scheme 1 outperforms Scheme 2 until around $P_d = 5$ dBm due to the scarcity of signal power, Scheme 2 outperforms Scheme 1 at higher transmit powers thanks to fewer pilots. Therefore, it can be inferred from Fig. 5 that given pure-LOS conditions between the BSs and the RISs, the baseline scheme is preferable over the two schemes when transmit power is limited. In contrast, Scheme 2 provides the best performance when the transmit power is high.

While there exists a region where baseline scheme prevails when pure-LOS RIS-BS channels exist, this is not the case when these channels do not exhibit any structure, as seen in Fig. 6. The two schemes that eliminate inter-operator pilot contamination consistently outperform the baseline scheme as the intended and the interfering channels are not well-separated over space. That is, pilot contamination has to be eliminated either at the RISs or the BS. Also, note that Scheme 2 outperforms both Scheme 1 and Scheme 2 almost everywhere in Fig. 6. Therefore, one can infer that Scheme 2 provides the best performance when the RIS-BS channels do not exhibit any structure. Moreover, the strong connection between the results in Sections A and B demonstrates that inter-operator pilot contamination is a strong limiting factor of spectral efficiency and must be addressed to make RISs feasible in multi-operator deployments. Table 8 summarizes the minimum number of pilots required for each scheme and whether the schemes eliminate inter-operator pilot contamination or not.

X. CONCLUSIONS

In this paper, we investigated the use of receive beamforming to combat inter-operator pilot contamination in RIS-aided wireless systems where two operators share a site and utilize different RISs to serve their respective users. We considered uplink channel estimation and data transmission and proposed using receive beamforming at the BSs to remove the interference coming from the other operator's RIS by placing a null towards the respective channel. We considered two different schemes. In Scheme 1, the BS beamforms towards its intended channel without placing a null towards the interfering channel. The RISs configurations during the pilot transmission phase are orthogonalized to eliminate inter-operator pilot contamination. In Scheme 2, a null is placed towards the interfering RIS-BS channel to cut off the interfering transmission and reflection path. As the inter-operator pilot contamination is removed at the BS, the RISs configurations are not orthogonalized, hence the number of pilots used in the channel estimation phase is halved. We investigated the performance of these two schemes when the RIS-BS channels are pure-LOS and when they are unstructured in terms of channel estimation MSE, the resulting capacity lower bounds under imperfect CSI and the ergodic capacities. Our numerical results show that at high transmit powers, Scheme 2 outperforms Scheme 1 and the baseline scheme in terms of capacity lower bound due to a lower number of pilots and matching channel estimation performance. While Scheme 2 prevails at high transmit powers for both pure-LOS and unstructured RIS-BS channel scenarios, this is not the case at low transmit powers. The extra energy captured by Scheme 1 and the baseline scheme gains importance when the transmit power is low. In addition, the baseline scheme uses half as many pilots as Scheme 1, and it is not affected much by the inter-operator pilot contamination when the RIS-BS channels are

TABLE 8: Summary of pilot use, spectral efficiency, and pilot contamination elimination for the three schemes when two operators utilize N-element RISs and $D + L = 3N$.

Scheme	Minimum L	SE Multiplier $\left(\frac{D}{D+L}\right)$	Pilot contamination eliminated?
Baseline	N	$2/3$	No
1	$2N$	$1/3$	Yes
2	N	$2/3$	Yes

pure-LOS. This is because, the baseline scheme beamforms towards its intended channel, inevitably reducing its gain from the interfering channel. In contrast, Schemes 1 and 2 consistently outperform the baseline scheme when the RIS-BS channels are unstructured since beamforming towards the intended channel does not reduce the gain from the interfering channel. In addition, we also showed that Scheme 2 consistently outperforms both schemes in such scenarios. Therefore, we can conclude that the proposed scheme to eliminate inter-operator pilot contamination by receive beamforming is highly beneficial at high transmission powers, and the cases where the baseline scheme prevails are limited to pure-LOS RIS-BS channels and low transmission powers.

Since in this work we focused on the idea of placing a null towards the interfering channel and eliminating pilot contamination, we kept the rest of the system model rather simple and tractable. However, further work can be done on how this scheme performs under different channel characteristics and when multiple users are served. In Section VIII, we provided the system model formulation for the multi-user case. However, further analysis is required to identify how to handle the multi-user beamforming problem. In addition, further analysis should be conducted for high-mobility scenarios. While the mobility of users does not affect the beamforming schemes directly – since beamforming is done based on the relatively static RIS-BS channels – time variation models of the channels should be incorporated into the channel estimation scheme. Another important extension is to incorporate hardware impairments into the problem to investigate the feasibility of the proposed pilot-contamination mitigation schemes, as it is shown to be a performance limiter in wireless communication systems [38]. The non-trivial dynamic between beamforming and hardware impairments within the context of mitigating inter-operator pilot contamination is also an important extension of this work. This dynamic can be seen in [39].

REFERENCES

[1] S. Yang and L. Hanzo, "Fifty years of MIMO detection: The road to large-scale MIMOs," *IEEE Communications Surveys & Tutorials*, vol. 17, no. 4, pp. 1941–1988, 2015.

[2] D. Gesbert, M. Kountouris, R. W. Heath, C.-b. Chae, and T. Salzer, "Shifting the MIMO paradigm," *IEEE Signal Processing Magazine*, vol. 24, no. 5, pp. 36–46, 2007.

[3] T. L. Marzetta, "Massive MIMO: An introduction," *Bell Labs Technical Journal*, vol. 20, pp. 11–22, 2015.

[4] F. Rusek, D. Persson, B. K. Lau, E. G. Larsson, T. L. Marzetta, O. Edfors, and F. Tufvesson, "Scaling up MIMO: Opportunities and challenges with very large arrays," *IEEE Signal Processing Magazine*, vol. 30, no. 1, pp. 40–60, 2013.

[5] E. Björnson and L. Sanguinetti, "Rayleigh fading modeling and channel hardening for reconfigurable intelligent surfaces," *IEEE Wireless Communications Letters*, vol. 10, no. 4, pp. 830–834, 2021.

[6] G. Fodor, N. Rajatheva, W. Zirwas, L. Thiele, M. Kurras, K. Guo, A. Tölli, J. H. Sorensen, and E. De Carvalho, "An overview of massive MIMO technology components in METIS," *IEEE Communications Magazine*, vol. 55, no. 6, pp. 155–161, 2017.

[7] J. Jeon, G. Lee, A. A. Ibrahim, J. Yuan, G. Xu, J. Cho, E. Onggosanusi, Y. Kim, J. Lee, and J. C. Zhang, "MIMO evolution toward 6G: Modular massive MIMO in low-frequency bands," *IEEE Communications Magazine*, vol. 59, no. 11, pp. 52–58, 2021.

[8] S. Zeng, B. Di, H. Zhang, J. Gao, S. Yue, X. Hu, R. Fu, J. Zhou, X. Liu, H. Zhang, Y. Wang, S. Sun, H. Qin, X. Su, M. Wang, and L. Song, "RIS-based IMT-2030 testbed for MmWave multi-stream ultra-massive MIMO communications," *IEEE Wireless Communications*, vol. 31, no. 3, pp. 375–382, 2024.

[9] D. G. Brennan, "Linear diversity combining techniques," *Proceedings of the IRE*, vol. 47, no. 6, pp. 1075–1102, 1959.

[10] J. Winters, "Optimum combining in digital mobile radio with cochannel interference," *IEEE Journal on Selected Areas in Communications*, vol. 2, no. 4, pp. 528–539, 1984.

[11] O. Frost, "An algorithm for linearly constrained adaptive array processing," *Proceedings of the IEEE*, vol. 60, no. 8, pp. 926–935, 1972.

[12] T. L. Marzetta, "Noncooperative cellular wireless with unlimited numbers of base station antennas," *IEEE Trans. Wireless Commun.*, vol. 9, no. 11, pp. 3590–3600, 2010.

[13] L. Sanguinetti, E. Björnson, and J. Hoydis, "Toward Massive MIMO 2.0: Understanding spatial correlation, interference suppression, and pilot contamination," *IEEE Trans. Commun.*, vol. 68, no. 1, 2020.

[14] J. Jose, A. Ashikhmin, T. L. Marzetta, and S. Vishwanath, "Pilot contamination and precoding in multi-cell TDD systems," vol. 10, no. 8, pp. 2640–2651, 2011.

[15] V. Saxena, G. Fodor, and E. Karipidis, "Mitigating pilot contamination by pilot reuse and power control schemes for massive MIMO systems," in *2015 IEEE 81st Vehicular Technology Conference (VTC Spring)*, pp. 1–6, 2015.

[16] A. Popovska Avramova and V. B. Iversen, "Radio access sharing strategies for multiple operators in cellular networks," in *2015 IEEE International Conference on Communication Workshop (ICCW)*, pp. 1113–1118, 2015.

[17] S. K. A. Kumar and E. Oughton, "Techno-economic assessment of 5G infrastructure sharing business models in rural areas," *Frontiers in Computer Science*, pp. 01–22, 2023. DoI: 10.3389/fcomp.2023.1191853.

[18] E. J. Oughton, K. Katsaros, F. Entezami, D. Kaleshi, and J. Crowcroft, "An open-source techno-economic assessment framework for 5G deployment," *IEEE Access*, vol. 7, pp. 155930–155940, 2019.

[19] E. J. Oughton and W. Lehr, "Surveying 5G techno-economic research to inform the evaluation of 6G wireless technologies," *IEEE Access*, vol. 10, pp. 25237–25257, 2022.

[20] M. S. B. Syed, H. M. Attaullah, S. Ali, and M. I. Aslam, "Wireless communications beyond antennas: The role of reconfigurable intelligent surfaces," *Engineering Proceedings*, vol. 32, no. 1, 2023.

[21] S. H. Zainud-Deen, "Reconfigurable intelligent surfaces for wireless communications," in *2022 39th National Radio Science Conference (NRSC)*, vol. 1, pp. 342–342, 2022.

[22] M. Rihan, A. Zappone, S. Buzzi, G. Fodor, and M. Debbah, "Passive versus active reconfigurable intelligent surfaces for integrated sensing and communication: Challenges and opportunities," *IEEE Network*, vol. 38, no. 3, pp. 218–226, 2024.

[23] C. Pan, H. Ren, K. Wang, J. F. Kolb, M. Elkashlan, M. Chen, M. Di Renzo, Y. Hao, J. Wang, A. L. Swindlehurst, X. You, and L. Hanzo, "Reconfigurable intelligent surfaces for 6G systems: Principles, applications, and research directions," *IEEE Communications Magazine*, vol. 59, no. 6, pp. 14–20, 2021.

[24] E. Ayanoglu, F. Capolino, and A. L. Swindlehurst, "Wave-controlled metasurface-based reconfigurable intelligent surfaces," *IEEE Wireless Communications*, vol. 29, no. 4, pp. 86–92, 2022.

[25] J. Das, P. Das, A. Chandra, B. P. S. Sahoo, S. K. Vankayala, and S. Yoon, "Reducing pilot overhead for channel estimation in RIS-assisted millimeter-wave systems," in *2023 IEEE International Conference on Electronics, Computing and Communication Technologies (CONECCT)*, pp. 1–6, 2023.

[26] G. Zhou, C. Pan, H. Ren, P. Popovski, and A. L. Swindlehurst, "Channel estimation for RIS-aided multiuser millimeter-wave systems," *IEEE Transactions on Signal Processing*, vol. 70, pp. 1478–1492, 2022.

[27] S. Kim and B. Shim, "Channel estimation for reconfigurable intelligent surface-aided mmwave communications," in *GLOBECOM 2022 - 2022 IEEE Global Communications Conference*, pp. 5396–5401, 2022.

[28] C. Pan, G. Zhou, K. Zhi, S. Hong, T. Wu, Y. Pan, H. Ren, M. D. Renzo, A. Lee Swindlehurst, R. Zhang, and A. Y. Zhang, "An Overview of Signal Processing Techniques for RIS/IRS-Aided Wireless Systems," *IEEE Journal of Selected Topics in Signal Processing*, vol. 16, no. 5, pp. 883–917, 2022.

[29] L. Wei, C. Huang, G. C. Alexandropoulos, C. Yuen, Z. Zhang, and M. Debbah, "Channel estimation for RIS-empowered multi-user MISO wireless communications," *IEEE Transactions on Communications*, vol. 69, no. 6, pp. 4144–4157, 2021.

[30] E. Björnson and P. Ramezani, "Maximum likelihood channel estimation for RIS-aided communications with LOS channels," in *Asilomar Conference on Signals, Systems and Computers*, 2022.

[31] C. Huang, A. Zappone, G. C. Alexandropoulos, M. Debbah, and C. Yuen, "Reconfigurable intelligent surfaces for energy efficiency in wireless communication," vol. 18, no. 8, pp. 4157–4170, 2019.

[32] D. Gürgünoğlu, E. Björnson, and G. Fodor, "Impact of pilot contamination between operators with interfering reconfigurable intelligent surfaces," in *2023 IEEE International Black Sea Conference on Communications and Networking (BlackSeaCom)*, pp. 27–32, 2023.

[33] D. Gürgünoğlu, E. Björnson, and G. Fodor, "Combating inter-operator pilot contamination in reconfigurable intelligent surfaces assisted multi-operator networks," *IEEE Transactions on Communications*, vol. 72, no. 9, pp. 5884–5895, 2024.

[34] N. I. Miridakis, T. A. Tsiftsis, P. A. Karkazis, H. C. Leligou, and P. Popovski, "Impact of inter-operator interference via reconfigurable intelligent surfaces," *IEEE Wireless Communications Letters*, vol. 13, no. 9, pp. 2536–2540, 2024.

[35] E. Björnson, H. Wymeersch, B. Matthiesen, P. Popovski, L. Sanguinetti, and E. de Carvalho, "Reconfigurable intelligent surfaces: A signal processing perspective with wireless applications," *IEEE Signal Processing Magazine*, vol. 39, no. 2, pp. 135–158, 2022.

[36] C. Hu, L. Dai, S. Han, and X. Wang, "Two-timescale channel estimation for reconfigurable intelligent surface aided wireless communications," *IEEE Transactions on Communications*, vol. 69, no. 11, pp. 7736–7747, 2021.

[37] T. L. Marzetta, E. G. Larsson, H. Yang, and H. Q. Ngo, *Fundamentals of Massive MIMO*. Cambridge University Press, 2016.

[38] Q. Li, M. El-Hajjar, Y. Sun, and L. Hanzo, "Performance analysis of reconfigurable holographic surfaces in the near-field scenario of cell-free networks under hardware impairments," *IEEE Transactions on Wireless Communications*, vol. 23, no. 9, pp. 11972–11984, 2024.

[39] Q. Li, M. El-Hajjar, Y. Sun, I. Hemadeh, A. Shojaeifard, and L. Hanzo, "Energy-efficient reconfigurable holographic surfaces operating in the presence of realistic hardware impairments," *IEEE Transactions on Communications*, vol. 72, no. 8, pp. 5226–5238, 2024.